THE GEOLOGICAL SOCIETY OF AMERICA®

A sudden end-Permian mass extinction in South China

Shu-Zhong Shen[1,2,†], Jahandar Ramezani[3], Jun Chen[4,†], Chang-Qun Cao[1], Douglas H. Erwin[5], Hua Zhang[1], Lei Xiang[1], Shane D. Schoepfer[6], Charles M. Henderson[7], Quan-Feng Zheng[1,8], Samuel A. Bowring[3], Yue Wang[1], Xian-Hua Li[9], Xiang-Dong Wang[2,8], Dong-Xun Yuan[1], Yi-Chun Zhang[1], Lin Mu[1,8], Jun Wang[1,2], and Ya-Sheng Wu[10]

[1]*State Key Laboratory of Palaeobiology and Stratigraphy, Nanjing Institute of Geology and Palaeontology and Center for Excellence in Life and Palaeoenvironment, Chinese Academy of Sciences, Nanjing 210008, China*

[2]*Centre for Research and Education on Biological Evolution and Environment, Nanjing University, Nanjing 210023, China*

[3]*Department of Earth, Atmospheric and Planetary Sciences, Massachusetts Institute of Technology, 77 Massachusetts Avenue, Cambridge, Massachusetts 02139, USA*

[4]*State Key Laboratory of Isotope Geochemistry, Guangzhou Institute of Geochemistry, Chinese Academy of Sciences, Guangzhou 510640, China*

[5]*Department of Paleobiology, MRC-121, National Museum of Natural History, Washington, D.C. 20013-7012, USA*

[6]*Department of Geosciences and Natural Resources, Western Carolina University, Cullowhee, North Carolina 28723, USA*

[7]*Department of Geoscience, University of Calgary, Calgary, Alberta, T2N 1N4 Canada*

[8]*CAS Key Laboratory of Economic Stratigraphy and Palaeogeography, Nanjing Institute of Geology and Palaeontology and Center for Excellence in Life and Palaeoenvironment, Chinese Academy of Sciences, Nanjing 210008, China*

[9]*State Key Laboratory of Lithospheric Evolution, Institute of Geology and Geophysics, Chinese Academy of Sciences, Beijing 100029, China*

[10]*CAS Key Laboratory of Petroleum Resource Research, Institute of Geology and Geophysics, Chinese Academy of Sciences, Beijing 100029, China*

ABSTRACT

Previous studies of the end-Permian mass extinction have established that it was geologically rapid, but condensed sections have made it difficult to establish the exact timing of the extinction relative to fluctuations in the ocean carbon cycle, oxygen levels, and temperature. Integrated high-precision U-Pb geochronology, biostratigraphy, and chemostratigraphy from a highly expanded section at Penglaitan, Guangxi, South China reveal a sudden end-Permian mass extinction that occurred at 251.939 ± 0.031 Ma, which is temporally coincident with the extinction recorded in Bed 25 of the Meishan section. Despite the significantly expanded nature of the section and extensive collecting of more than ten major marine fossil groups, there is no evidence of a decline of biotic diversity prior to the extinction interval and no Permian-type species survive the extinction at this location. Fossil range data suggest a nearly instantaneous extinction at the top of a narrow stratigraphic interval limited to 31 ± 31 k.y. The extinction was preceded by and/or accompanied by fluctuations in $\delta^{13}C_{carb}$ and $\delta^{13}C_{org}$ of 2–3‰, and 3–5 °C in seawater temperature. A larger, more rapid seawater temperature rise of 6–8 °C immediately followed the extinction level at Penglaitan. The extinction is spatially associated with a thick unit of tuff and tuffaceous sandstones (Bed 141) indicating massive pyroclastic input. It is correlative with an ash layer (Bed 25) in the deeper water setting at Meishan, where some Permian-type organisms survived the extinction. Our study reveals that the survivability of Permian taxa after the major extinction pulse is variable and dependent upon the severity of environmental perturbation in different sedimentary settings. The sudden extinction may fit a scenario in which the onset of Siberian Traps and South China intensive volcanism ~420 k.y. before the extinction may have diminished the ecological resilience of communities and reduced ecological functions with little change in diversity. In such an environmentally stressed condition, a single environmental disturbance could trigger the sudden collapse of global ecosystems.

INTRODUCTION

The complex, multi-causal end-Permian mass extinction (EPME) was associated with major environmental perturbations over a short time interval, yet despite intensive recent studies, questions about the exact patterns and timing of the extinction remain unresolved (e.g., Shen and Bowring, 2014). Currently one of the crucial data sets used to unravel the extinction is from the Global Stratotype Section and Point (GSSP) of the Permian-Triassic boundary (PTB) at the Meishan section in South China. However, the extinction interval corresponding to Beds 25–28 at Meishan is highly condensed (only 0.36 m thick) and may also contain multiple depositional hiatuses at or below the PTB (Cao and Zheng, 2007, 2009; Zheng et al., 2013). The condensed nature of the section may have masked the detailed record of biotic change and eliminated evidence of environmental deterioration prior to the extinction episode. This combination of condensation and hiatuses imposes inherent limits in temporal resolution for the interpretations of complex biotic and environmental signals from the end-Permian sedimentary record (Cao et al., 2009; Xie et al., 2007).

Numerous age-calibrated, statistical analyses of abundant fossil evidence support a single, brief catastrophic end-Permian extinction (Burgess et al., 2014; Jin et al., 2000; Rampino et al., 2000; S.Z. Shen et al., 2011a; Wang et al., 2014), in contrast to other studies suggesting two or more extinction pulses near the PTB (Song et al., 2009, 2013; Yin et al., 2012). These different interpretations cannot be resolved within condensed sections like Meishan. Expanded PTB sequences documented from the

†Corresponding authors: szshen@nigpas.ac.cn, junchen@gig.ac.cn.

GSA Bulletin; January/February 2019; v. 131; no. 1/2; p. 205–223; https://doi.org/10.1130/B31909.1; 13 figures; 1 table; Data Repository item 2018201; published online 19 September 2018.

Gartnerkofel-1 core and other sections in the Alps also appear to record a catastrophic event (Brand et al., 2012; Holser et al., 1989; Perri and Farabegoli, 2003; Posenato, 2010; Rampino et al., 2000). However, no high-precision geochronologic dates have been reported from the Gartnerkofel-1 core, nor is there sufficient paleontological data for statistical analysis. Other sections more expanded than Meishan have been reported from East Greenland and Spitsbergen (Grasby et al., 2015; Twitchett et al., 2001; Wignall and Twitchett, 2002), the Canadian Arctic (Algeo et al., 2012; Grasby and Beauchamp, 2009), the Salt Range of Pakistan (Pakistani-Japanese Working Group, 1985) and Kashmir (Brookfield et al., 2003). The extinction interval in these sections varies from a few to ~20 m. However, all lack high-precision age constraints; some sections have disconformities similar to those observed at Meishan (Hays et al., 2012; Hermann et al., 2010) or include an impoverished pre-extinction fauna.

A section with higher sedimentation rates and better geochronologic (Burgess et al., 2014) and stratigraphic (Yuan et al., 2014) controls, as well as paleontological data comparable to Meishan (Jin et al., 2000; S.Z. Shen et al., 2011a; Wang et al., 2014) would provide the opportunity to analyze the fine structure of the extinction. Such a setting would allow determination of the extinction rate and its relationship to coeval environmental perturbations. Here we report biostratigraphic, chemostratigraphic and geochronologic data from such an expanded PTB section from Penglaitan near Laibin City, South China (Fig. 1). New high-precision U-Pb geochronology from seven closely spaced tuff and tuffaceous sandstones coupled with detailed biostratigraphy throughout the Penglaitan section reveal that the Changhsingian and PTB interval are >100 times thicker than at Meishan (Fig. 2). Therefore, the Penglaitan section provides an unprecedented stratigraphic resolution and a unique opportunity to resolve the tempo and pattern of the most severe mass extinction in Earth history and its associated biotic and environmental perturbations. Moreover, such high resolution allows us to evaluate the occurrence of potential signals of early environmental degradation and biotic collapse.

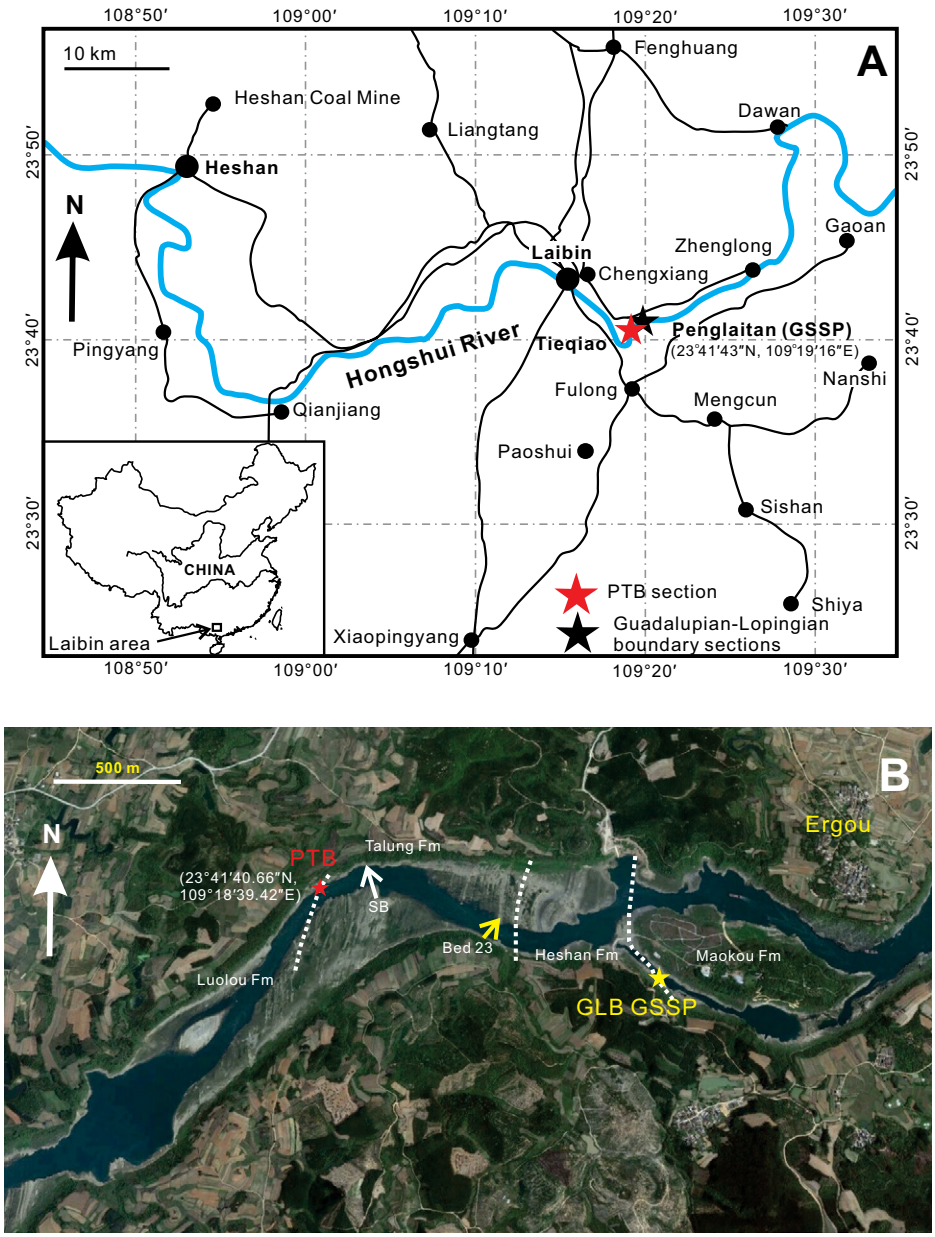

Figure 1. (A) Location map of the Lopingian-base Global Stratotype Section and Point (GSSP) and the Penglaitan section in the Laibin area, Guangxi Province, South China. (B) Google Earth image of the Permian-Triassic boundary (PTB) section at Penglaitan and its main lithostratigraphic boundaries along the northern bank of the Hongshui River. GLB—Guadalupian-Lopingian boundary.

GEOLOGICAL SETTING AND BIOSTRATIGRAPHY OF THE PENGLAITAN SECTION

Penglaitan was situated near the eastern (Heshan) carbonate platform of the Late Permian-Middle Triassic Nanpanjiang Basin, which formed a deep-marine embayment along the southern margin of the South China Block (Lehrmann et al., 2005). The Permian-Triassic record of the basin is consistent with tectonic convergence and magmatic arc development to the south (He et al., 2014; Yang et al., 2012). The Penglaitan section has been used to define the base of the Lopingian Series (Jin et al., 2006) and preserves the complete Lopingian Series of South China (Jin et al., 1998; Shen et al., 2010). This succession is continuously exposed for 1.3 km along the banks of the Hongshui River, ~20 km southeast of Laibin City (Fig. 1). Abundant fossils have been recovered and the ranges of conodonts, fusulinids, foraminifers, ammonoids, brachiopods, bivalves, bryozoans, rugose corals, and plants have been determined.

The Lopingian Series at Penglaitan (Fig. 2) consists of (in ascending order) the uppermost part of the Maokou Formation, the Heshan Formation, and the remarkably thick Talung Formation, overlain by the uppermost Permian and Lower Triassic Luolou Formation (Shen et al., 2007). The Talung Formation is subdivided

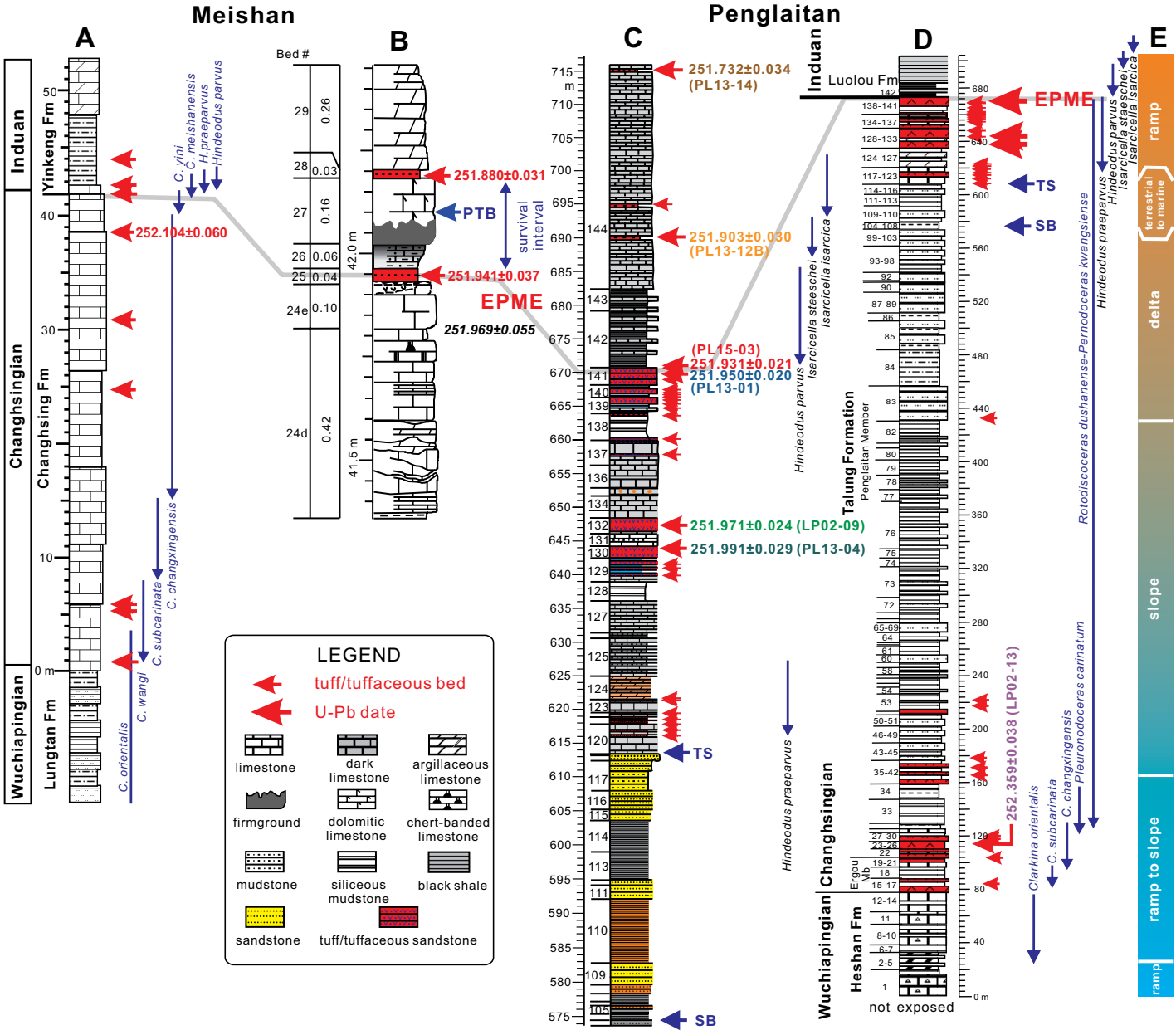

Figure 2. Correlation of the Permian-Triassic strata between the Meishan Global Stratotype Section and Point (GSSP) (A–B) and the Penglaitan section (C–E) in South China, including assigned bed numbers. Sections are shown in various scales. Stratigraphic ranges of conodont species are shown to the right of each column (except B). Columns B and C are respectively the zoomed-in Permian-Triassic boundary (PTB) intervals of A and D. Column E is the interpretation of the sedimentary environment of the Penglaitan section. Meishan stratigraphy is from S.Z. Shen et al. (2011a), and geochronology from Burgess et al. (2014). Our U-Pb geochronology is color-coded (see Fig. 5). The end-Permian mass extinction (EPME) at Bed 25 of Meishan and its correlation with Bed 141 at Penglaitan is highlighted by the gray line. SB—sequence boundary; TS—transgressive surface.

into two members. The lower Ergou Member is composed of silicified carbonate rocks and contains diverse ammonoids belonging to the lower Changhsingian *Penglaites* Zone (Ehiro and Shen, 2010). The overlying Penglaitan Member is very thick (523.6 m) and likely is the results of high rates of tectonic subsidence, associated with local syn-sedimentary faulting and abundant input of siliciclastic and pyroclastic materials from nearby arc-related volcanic eruptions. Its base is marked by a resistant bed of coarse tuffaceous sandstone. The uppermost part of the formation consists primarily of mixed carbonate-clastic turbidites or storm deposits with more than 50 massive, immature tuffs and tuffaceous sandstones interbedded with carbonates. The lowest strata of the Luolou Formation are characterized by a fissile black shale with centimeter-scale limestone interbeds, containing abundant fossils of the Triassic bivalve *Claraia*, numerous microgastropods and the conodont *Hindeodus parvus* (Fig. 3). This black shale interval is overlain by thin-bedded limestone containing *Isarcicella* species and a few tuffaceous

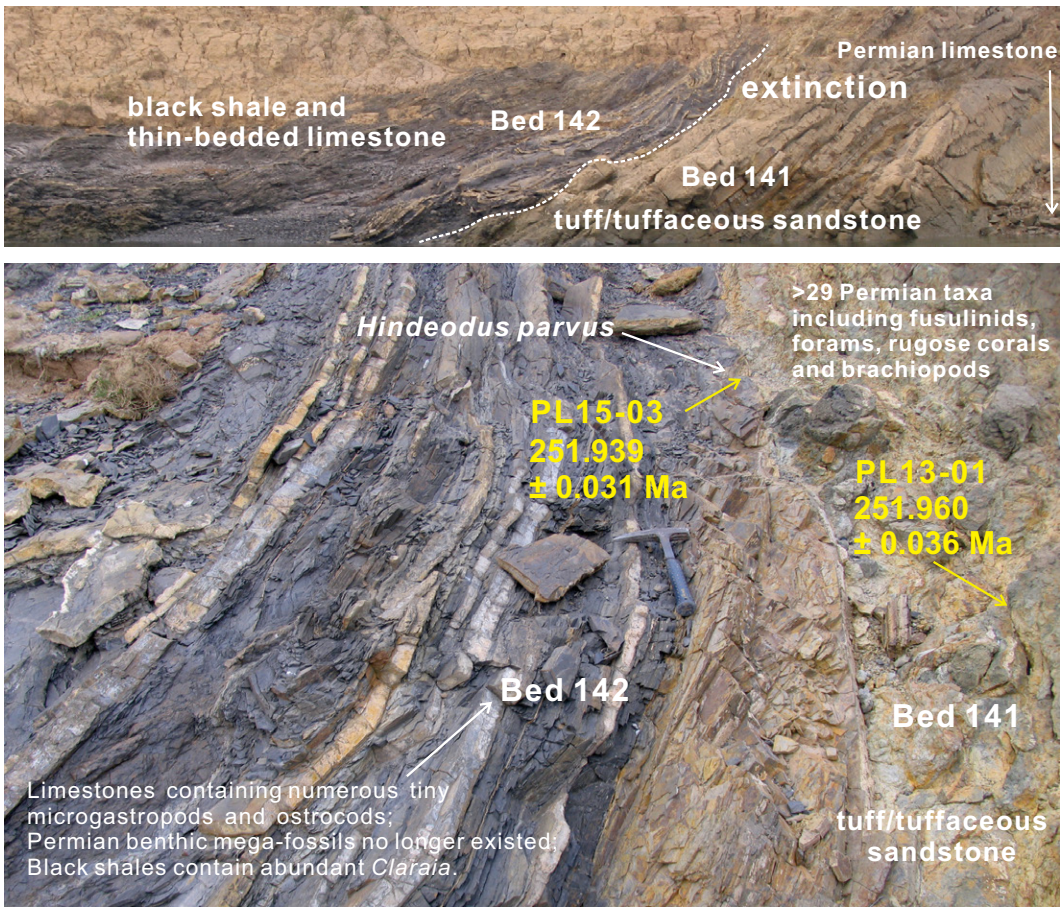

Figure 3. Outcrop photos of the Permian-Triassic boundary interval at Penglaitan showing from right to left the uppermost Permian tuffs/tuffaceous sandstones (Bed 141), the extinction horizon (dashed line, hammer), and the basal Triassic black shales with interbedded limestones (Bed 142). Our U-Pb ages (yellow) are from the actual measured dates (see Table 1), and differ from interpolated dates shown in Figures 2, 4, and 10.

beds in the basal part of the Lower Triassic (Figs. 2, 4) succession. The biostratigraphically defined EPME horizon (see "Fossil Extinction Pattern" below) is located at 670.72 m above the base of the measured Penglaitan section at the top of Bed 141 (Figs. 2–4), which coincides with the top of the Penglaitan Member.

U-Pb GEOCHRONOLOGY OF THE PTB INTERVAL AND DURATION OF MASS EXTINCTION

Multiple samples of tuff and tuffaceous sandstone were collected from a 74 m stratigraphic interval at Penglaitan spanning the uppermost Changhsingian Stage of Permian to the lower Induan Stage of the Lower Triassic. Five samples (PL13-04, PL13-01, PL15-03, PL13-12B, and PL13-14) were targeted for zircon geochronology based on the yield and state of preservation of the zircon crystals, and analyzed for U and Pb isotopes using the chemical abrasion–isotope dilution–thermal ionization mass spectrometry (CA-ID-TIMS) technique (Figs. 2–5). In addition, a tuff sample (LP02-13) from the basal part of the Penglaitan Member (Bed 23 at 108.2 m) and another (LP02-09) from Bed 132 at 648.4 m, which had been previously dated by the U-Pb CA-ID-TIMS method (S.Z. Shen et al., 2011a) but using different analytical protocols and isotopic tracer, were re-analyzed in this study (Table 1). Details of analytical procedures including an optimized CA-TIMS schedule and the use of EARTHTIME isotopic tracer, as well as data reduction and age calculation strategies are given in the GSA Data Repository.[1] Complete U and Pb isotopic data for 80 zircon analyses are listed in Table DR1 (see footnote 1). Summary of calculated ages and uncertainties at 95% confidence level can be found in Table 1 and in the date distribution plots of Figure 5.

Our new geochronology provides a high-resolution framework for the tempo of the EPME at Penglaitan. The set of seven high-precision U-Pb dates span less than 700 k.y. over 608 m of strata, attesting to the remarkably high sediment accumulation rates at Penglaitan during the Permian-Triassic transition. As a result, the U-Pb dates that most closely bracket the extinction—from 643.5 m (PL13-04, Bed 130) to 690.0 m (PL13-12B, Bed 144)—display a significant degree of overlap within the analytical uncertainties (Fig. 5). Some of the dated tuffs that straddle the extinction horizon produced more objective weighted mean $^{206}Pb/^{238}U$ dates than others (see explanation in Data Repository), because of the absence or paucity of detrital zircons in the analyses (e.g., samples PL13-04 and PL15-03). Linear extrapolation between the latter dates results in an age of 251.939 ± 0.031 Ma for the extinction horizon and a duration of 31 ± 31 k.y. for the EPME. A similar extrapolation between samples PL15-03 (Bed 142) at 670.92 m and PL13-12B (Bed 144) at 690.0 m places the first occurrence (FO) of *Hindeodus parvus* at Penglaitan at 251.939 ± 0.031 Ma, which is indistinguishable from the age of the extinction.

The set of six closely spaced, high-precision U-Pb dates from the Talung and Luolou formations on either side of the mass extinction level allows us to employ a Bayesian age-depth model to further refine the chronostratigraphy. The analyses of our tuff dates, their uncertainties and exact stratigraphic levels through the Bchron package (Haslett and Parnell, 2008; Parnell et al., 2008) results in new interpolated ages

[1]GSA Data Repository item 2018201, Methods, zircon U-Pb, $\delta^{13}C_{carb}$, $\delta^{18}O_{carb}$, $\delta^{13}C_{org}$, TOC (total organic carbon), and $\delta^{18}O_{apatite}$ data, is available at http://www.geosociety.org/datarepository/2018 or by request to editing@geosociety.org.

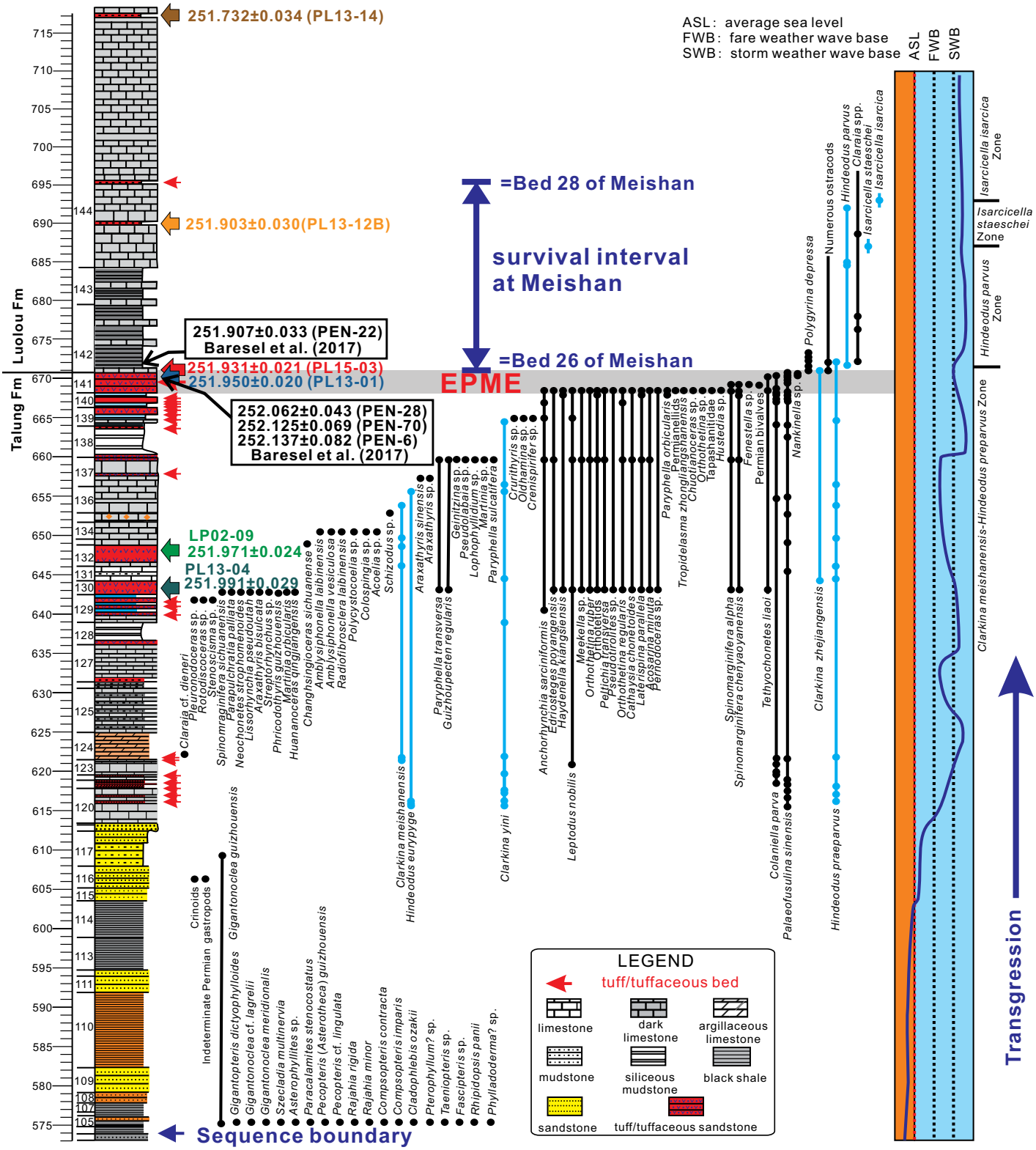

Figure 4. Detailed fossil ranges and conodont zones in the uppermost Changhsingian and lowermost Triassic of the Penglaitan section and their correlation with the extinction and survival interval of the Meishan section (in dark blue). Conodont ranges are marked in light blue. Geochronological dates from Baresel et al. (2017) are shown in black boxes. Interpreted sea-level changes are shown on the right column. EPME—end-Permian mass extinction. See Figure 5 for details of our U-Pb dates (color-coded).

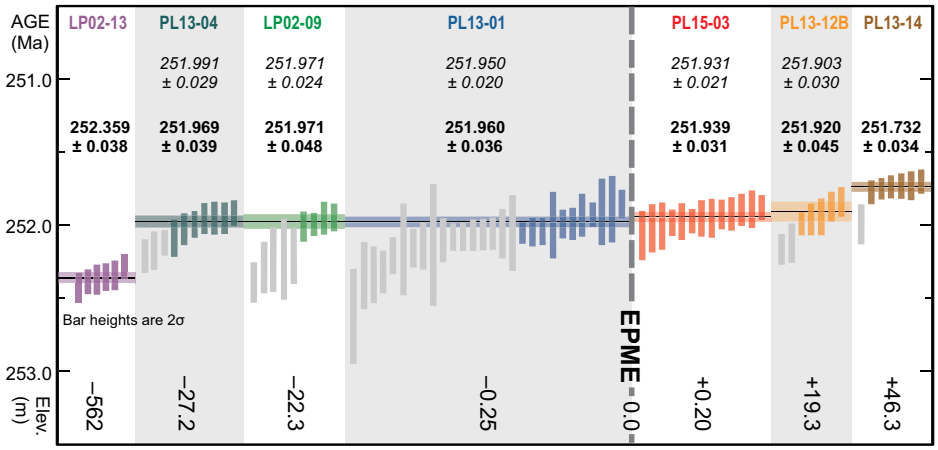

Figure 5. Date distribution plots for the analyzed zircons from the Permian-Triassic samples of the Penglaitan section (color-coded). Bar heights are proportional to 2σ analytical uncertainty of individual analyses; gray bars are older detrital/xenocrystic analyses excluded from weighted mean date calculation. Horizontal lines signify calculated sample dates and the width of the shaded band represents internal uncertainty in the weighted mean date at 95% confidence level. Two sets of dates are shown, which correspond to the actual calculated weighted mean $^{206}Pb/^{238}U$ dates (in bold) and their 2σ internal uncertainties (Table 1), and to the interpolated dates for each level from the Bayesian age-depth modeling (in italics). The latter set is that shown in Figures 2, 4, and 10. See GSA Data Repository (footnote 1) for Bchron interpolations. Stratigraphic distances from the extinction horizon (0.0 = 670.72 m) are shown along the bottom. EPME—end-Permian mass extinction.

for each tuff level (see Fig. 5), as well as the extinction horizon (see Data Repository for details). The new age-depth model constrains the extinction level at 251.940 ± 0.019 Ma and with a duration of 19 +29/–19 k.y. The results from both linear and Bayesian models are nearly identical, although the latter generates notably smaller uncertainties.

It is difficult to unequivocally quantify sediment accumulation rates over short stratigraphic intervals at Penglaitan because of overlap between the adjacent ages and the resulting high uncertainties in Δt. Nevertheless, the average sediment accumulation rates for the upper 27 m of the Talung Formation is 69 cm/k.y. in contrast to those for the lower 46 m of the Luolou Formation, which is on the order of 22 cm/k.y. Sharp changes in the deposition rate occur in association with large tuffaceous accumulations. Our results rule out any major unconformity at the Talung/Luolou formational boundary. If any depositional gap occurred at this boundary, its magnitude was likely smaller that the ~± 0.04 m.y. analytical uncertainty of our CA-ID-TIMS ages.

FOSSIL EXTINCTION PATTERN

The uppermost Changhsingian at Penglaitan includes one of the most diverse latest Permian faunal assemblages yet described. It consists of at least ten major marine fossil groups and at least 66 identified marine species including 38 brachiopod species (Fig. 4), eight Permian ammonoid species, six calcisponge species, one rugose coral (*Lophophylidium* sp.), five conodonts (Fig. 6), four abundant foraminifers (*Palaeofusulina sinensis*, *Nankinella* sp., *Colaniella parva*, *Geinitzina* sp.) (Fig. 7), two Permian-type bivalves (*Guizhoupecten regularis*, *Schizodus* sp.), one Triassic-type (*Claraia* cf. *dieneri*) taxon (Fig. 8), one abundant Permian bryozoan (*Fenestella* sp.), some trilobites, as well as gastropod and crinoid fragments (Fig. 4). This diversity is well above that recorded in most of the EPME intervals elsewhere. The possibility of significant fossil reworking in the topmost part of the extinction horizon (Bed 141) from the underlying carbonate and tuffaceous beds can be ruled out because all micro- and megafossils are relatively complete and free of debris or matrix (Figs. 7G–L, 9F).

Our collections of major marine fossil groups from the Penglaitan section are composed of Permian-type taxa except for the bivalve *Claraia* cf. *dieneri*, which indicates that presumed Triassic progenitors can occur earlier than previously documented (Sheng et al., 1984). The last occurrences (LOs) of all Permian species, including such major fossil groups as foraminifers, brachiopods, rugose corals, and reef-building sponges, fall within a 27.4 m interval between Bed 130 (643.5 m) and the top of the last thick tuffaceous sandstone unit (Bed 141, 670.72 m) (Figs. 3, 4). Among the 66 identified marine species, 29 species disappear within or at the top of the Bed 141, suggesting a highly diverse Permian benthic community continued to be present until Bed 141. Thirty-five species disappear between Beds 130 and 140 and two (*Hindeodus praeparvus* and *Claraia* cf. *dieneri*) extended into the earliest Triassic (Fig. 4). Thin-sections (Fig. 7M) from the thin-bedded limestone ~20 cm above the top of Bed 141 reveal numerous microgastropods (*Polygyrina depressa*), fragmentary bivalve shells and no typical Permian-type benthic megafossils. This highlights a dramatic replacement of the end-Permian benthic community by a new assemblage containing only Triassic conodonts and opportunistic taxa (ostracods and microgastropods). Lower in the Penglaitan section, tuffaceous turbidites or debris flows appear to have temporarily disrupted the local environments, but in each case the ecology was reestablished with the return of normal carbonate deposition. This did not occur above Bed 141. The survival of some Permian taxa into the basal Triassic has been documented from many other sections (e.g., until Bed 28 at Meishan) (Sheng et al., 1984), which was interpreted as a second phase of extinction at Bed 28 (Song et al., 2013).

TABLE 1. SUMMARY OF CALCULATED U-Pb AGES AND THEIR UNCERTAINTIES

Sample	Formation	Bed no.	Above base*	Stratigraphic horizon†	$^{206}Pb/^{238}U$ age	Uncertainty (2σ) X§	Y#	Z**	MSWD††	n§§
PL13-14	Luolou	144	717.0	+46.3	251.732	0.034	0.074	0.28	0.36	6
PL13-12B	Luolou	144	690.0	+19.3	251.920	0.045	0.080	0.28	1.8	5
PL15-03	Luolou	142	670.92	+0.20	251.939	0.031	0.073	0.28	0.77	13
Extinction Horizon		141	670.72	0.00						
PL13-01	Talung	141	670.47	–0.25	251.960	0.036	0.075	0.28	1.5	10
LP02-09	Talung	132	648.4	–22.3	251.971	0.048	0.081	0.28	0.42	4
PL13-04	Talung	130	643.5	–27.2	251.969	0.039	0.077	0.28	1.1	7
LP02-13	Heshan	23	108.2	–562	252.359	0.038	0.076	0.28	1.2	6

*Meters above base of exposed section at Penglaitan.
†Meters from top of extinction horizon at 670.72 meters above base.
§X—internal (analytical) uncertainty in the absence of all external or systematic errors.
#Y—incorporates the U-Pb tracer calibration error.
**Z—includes X and Y, as well as the uranium decay constant errors.
††MSWD—mean square of weighted deviates.
§§*n*—number of analyses included in the calculated weighted mean date.

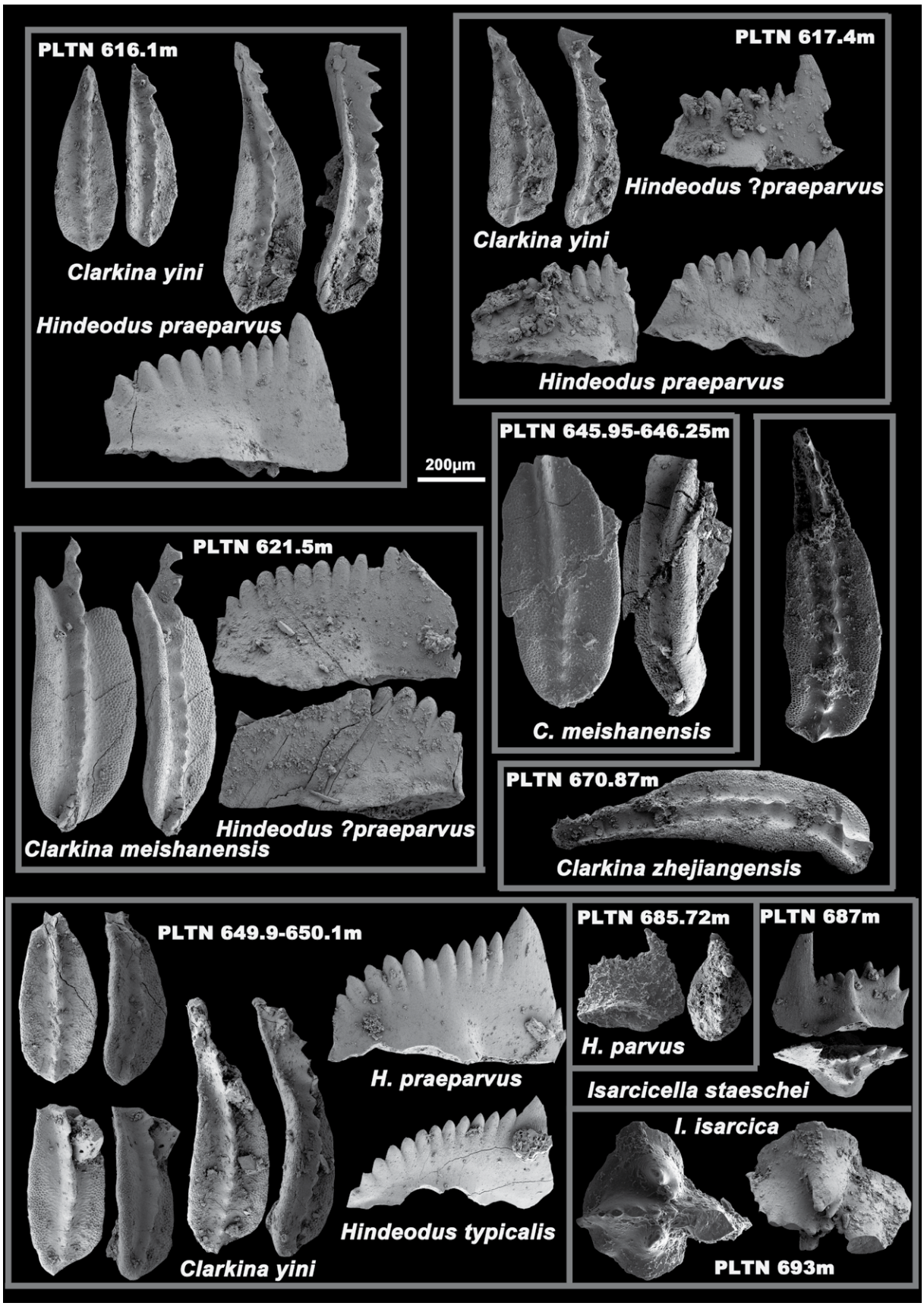

Figure 6. Conodonts from the Permian-Triassic boundary interval at the Penglaitan section.

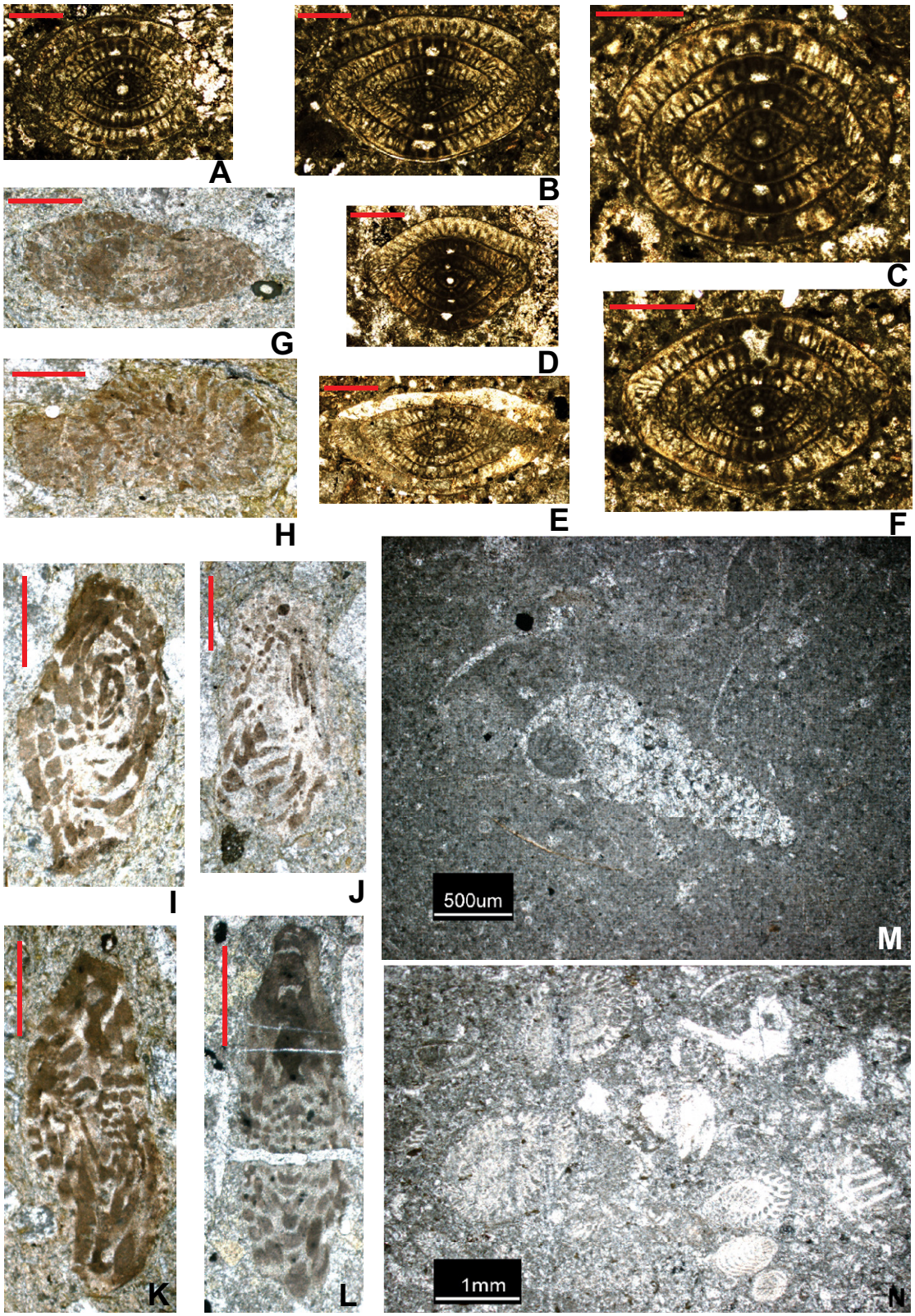

Figure 7. Photomicrographs of fusulinids and microgastropods from the Permian-Triassic boundary interval at the Penglaitan section. (A–H) *Palaeofusulina sinensis*; (A–D, F) from Bed 136; (E) from Bed 133; (G, H) from 670.13 to 670.54 m in Bed 141; (I–L) *Nankinella* sp. from 670.13 to 670.54 m in Bed 141; (M) a tiny gastropod which is very abundant in the thin-bedded limestones in Bed 142; (N) abundant *Palaeofusulina sinensis* and *Colaniella parva* at 667.54 m. (A–F, I) axial sections; (G, J) tangential sections; (H) transverse section. Scale bars for A–L are 500 μm; for M and N as indicated.

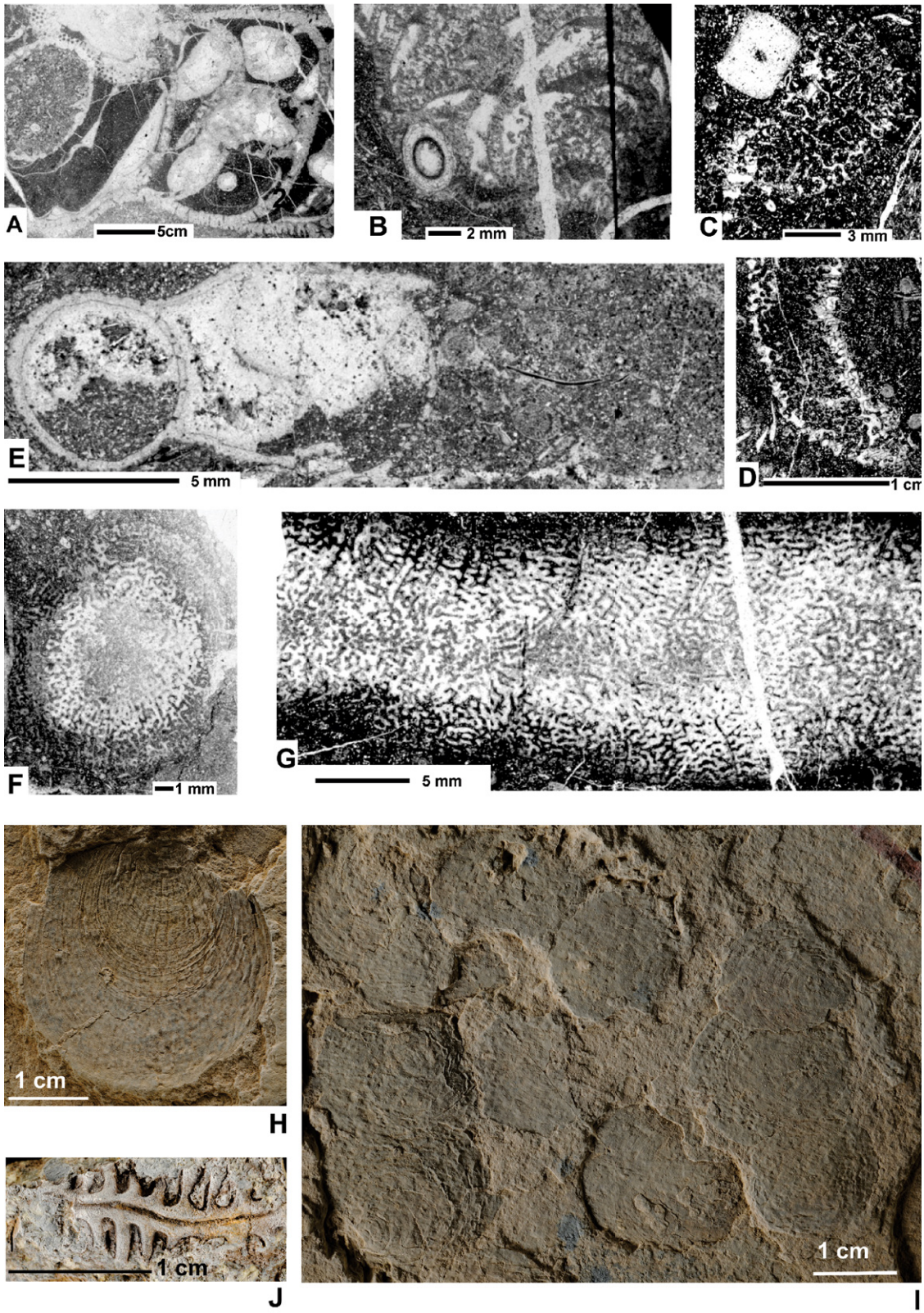

Figure 8. Photographs of some Penglaitan fossils, including sponges from Bed 132 and *Claraia* aff. *dieneri* from Bed 124. The high abundance of *Claraia* in some horizons suggests that pioneering organisms began to populate stressful environments during and before the mass extinction. (A) *Amblysiphonella vesiculosa* Koninck; (B) *Polycystocoelia* sp.; (C, D) *Acoelia* sp.; (E) *Colospongia* sp., longitudinal section; (F, G) *Retinospongea*, new taxon; (H, I) *Claraia* aff. *dieneri*, from Bed 124; (J) *Leptodus nobilis*, from the uppermost part of Bed 141, a typical Permian brachiopod seen in normal marine environments.

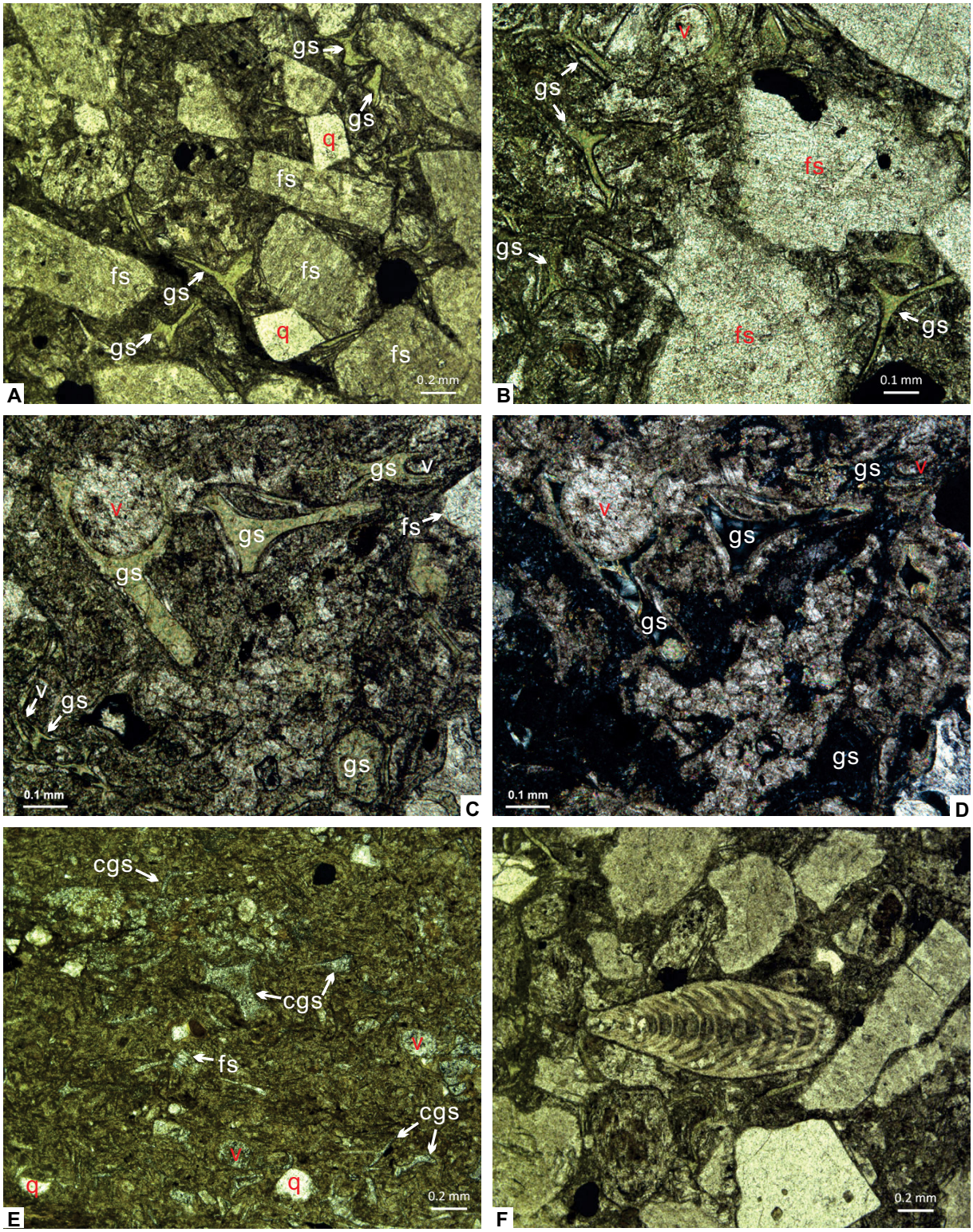

Figure 9. Photomicrographs of the Bed 141 tuffs in thin section, showing their mineralogic composition and texture. (A) Crystal tuff in the lower part of Bed 141, with phenocrysts of mainly plagioclase feldspars (fs), with subordinate quartz (q) and glass shards (gs) in plane-polarized light (PPL). (B) Crystal-vitric tuff from the lower part of Bed 141 showing glass shards and calcite-filled vesicles (v), in PPL. (C) PPL and (D) cross-polarized light volcanic glass shards partly replaced by chlorite developed in the crystal-vitric tuff in the lower part of Bed 141, with calcite infillings of larger vesicles. (E) Vitric tuff from the uppermost part of Bed 141, showing minor volcanic clasts of mainly quartz and feldspar, together with partially calcified glass shards (cgs) in PPL. (F) A well-preserved small foraminifer *Colaniella parva* within the crystalline tuff of lower Bed 141, in PPL.

However, the Penglaitan section does not contain a "survival interval" of Permian taxa extending into the Early Triassic. This indicates that the effects associated with global environmental perturbation more severely affected the shallower depositional setting represented in Bed 141 at Penglaitan compared to that at Meishan in the equivalent Bed 25.

The observed disappearance of taxa over an extended stratigraphic interval can be interpreted in one of multiple ways: (*a*) a true stepwise extinction occurred within the 27.4 m interval, meaning that the collected data serve as a reliable and complete record of biotic change (Fig. 4); (*b*) the observed sequential disappearances is caused by incomplete preservation and the backward-smearing Signor-Lipps effect, pointing to a much more rapid extinction pulse coincident with the volcanic eruption event in Bed 141 (Fig. 3); (*c*) insufficient collecting of fossils, or (*d*) strong taphonomic control because of lithofacies changes.

The most parsimonious interpretation of the data is an extinction within the time of deposition of Bed 141 since the default assumption must be the presence of a Signor-Lipps effect, based on the sudden changeover from the Permian benthic community to the Triassic bivalve and gastropod-dominated community and the sharp lithologic changes below and above Bed 141 (Fig. 3). Our U-Pb geochronologic results from bracketing tuff samples constrains the duration of the EPME at the top of Bed 141 to within 31 ± 31 k.y. (or 19 +29/–19 k.y. based on Bchron age-depth modeling). This temporal resolution is limited by the precision of our dating technique. Considering the stratigraphic and sedimentologic evidence for a narrow extinction interval at the top of Bed 141, it is likely that the extinction occurred much more rapidly than our estimates and was instantaneous by geologic measures.

PETROLOGIC EXAMINATION OF THE TUFFACEOUS SANDSTONE AT THE EXTINCTION INTERVAL

The upper 562 m of the Permian (i.e., Bed 23 to PTB) with a time span of 420 k.y. at the Penglaitan section contain more than 50 tuff or tuffaceous sandstone beds, documenting two episodes of accelerated volcanism near the base and top of the Penglaitan Member (Fig. 2D). The greater number of volcanic beds at Penglaitan relative to Meishan and many other sections in South China suggest Penglaitan was closer to the volcanic-arc eruption centers. One such bed is the ~2.5-m-thick Bed 141 that preserves the EPME near its top. It consists predominantly of tuffaceous sandstones, interbedded with more bentonitic layers up to several tens of centimeters in thickness. Detailed petrographic examination indicates that Bed 141 exhibits normal grading from a coarse-grained, crystal-vitric tuff to a fine vitric-ash tuff (Fig. 9). The basal lithology is mainly composed of coarse, plagioclase-dominated feldspars (56%–70%), subordinate quartz phenoclasts, and glass shards (Fig. 9A). Quartz phenoclasts commonly exhibit resorption embayments, and glass shards are associated with abundant vesicles. Most glass shards are replaced by chlorite and appear pale-green in plane-polarized light (Fig. 9A–9C). The uppermost 0.2 m of Bed 141 is a vitric ash tuff (Fig. 9E) with quartz, feldspar, glass shards, and minor volcanic clasts. Vesicles are commonly filled with calcite. Well-preserved and sometimes broken shallow-marine fossils occur sparsely in Bed 141 (Fig. 9F). The lithofacies of Bed 141 is consistent with relatively rapid deposition of large volumes of pyroclastic material from nearby volcanic eruptions in a shallow littoral or onshore coastal environment. It can be deduced that the voluminous pyroclastic flow swept across the shallow marine setting, where it entrained biologic material, before being deposited in an offshore ramp environment. Such deposits form more rapidly than the underlying carbonate or siliciclastic sediments. Nevertheless, the presence of clay-rich tuff interlayers suggests that pyroclastic deposition was interrupted by relatively calm episodes.

$\delta^{13}C_{carb}$ AND $\delta^{13}C_{org}$ EXCURSIONS

A sharp negative shift in carbon isotopes associated with the EPME has been documented globally (Korte and Kozur, 2010). At Meishan, the onset of a gradual decline in $\delta^{13}C_{carb}$ of 2‰ began ~60 k.y. prior to the extinction (in the middle part of Bed 23) (Burgess et al., 2014). This is followed by an abrupt 3‰–5‰ decline in $\delta^{13}C_{carb}$ marking the extinction at Beds 24e-25, which is estimated to have lasted <10 k.y. Further resolution of the $\delta^{13}C_{carb}$ record is impossible due to stratigraphic condensation and hiatuses, but the equivalent interval would be over 10 m thick at Penglaitan. To resolve these trends in greater detail, a total of 321 samples were analyzed for $\delta^{13}C_{carb}$ and $\delta^{18}O_{carb}$ from the entire Lopingian, and 77 samples from the uppermost 72 m of the Changhsingian and the basal Triassic for $\delta^{13}C_{org}$ and TOC (Fig. 10; Table DR2 [see footnote 1]).

Our results show a distinct negative shift of ~4‰–5‰ in the middle Wuchiapingian, which is comparable to some other sections in South China (Shen et al., 2013). $\delta^{13}C_{carb}$ values recovered to ~4‰ in the late Wuchiapingian to early Changhsingian, followed by two ~2‰ depletions. One is near the Wuchiapingian/Changhsingian boundary and the other coincides with Bed 22, the first massive volcanic eruption at Penglaitan (252.359 ± 0.038 Ma, 108.2 m) (Fig. 10; Table DR2). The second, relatively minor negative excursion is close to, but slightly earlier than the onset of $\delta^{13}C_{carb}$ decline in the middle part of Bed 23 at Meishan based on geochronologic and biostratigraphic constraints. At Penglaitan, this excursion is followed by a long interval with lower $\delta^{13}C_{carb}$ values within the –1‰ to +1‰ range, until the end of the extinction at 251.939 ± 0.031 Ma (670.72 m). Three positive excursions (PT-P 1-3) and two negative excursions (PT-N 1-2) at the 2‰–3‰ (between 1‰ and –2.5‰) level are present between 605 and 680 m (Fig. 10B, 10C).

A general negative excursion across the PTB has been globally recognized by previous studies, however, its magnitude and pattern are variable in different sections (Cao et al., 2010; Korte and Kozur, 2010; Shen et al., 2013). At Meishan, this excursion involves a gradual decline followed by a sharp negative shift in the extinction interval (Burgess et al., 2014; Cao et al., 2002, 2009; Shen et al., 2013; Xie et al., 2007). The sharpness of the negative shift reflects condensation—a comparable shift, if spread out over a significant thickness would not appear to be as sharp. In contrast, $\delta^{13}C_{carb}$ exhibited a long gradual decline at the Chaotian section in Sichuan and the Xishan section in Jiangsu in South China (Cao et al., 2010). One feature of the $\delta^{13}C_{carb}$ profile at Penglaitan which differs from other sections is a long interval with relatively low values (from 1‰ to –2.5‰) (Fig. 10B, 10C). The current evidence does not allow us to distinguish between alternative explanations for this pattern. One possibility is chaotic fluctuations in the carbon cycle before the extinction, reflecting complex local dynamics in proximal shallow water and terrestrial facies. However, values in the lowest tuffaceous unit (Beds 23–26) and the uppermost part of the section (Beds 117–140) in bioclastic carbonates should reflect open ocean conditions with no more depositional or diagenetic effects than in any other section. In between, the values are found in cements of deep sea sediments and in some terrestrial influenced units. These "in between" values remain relatively stable for the entire interval in the last 420 k.y. (Fig. 10A, 10B).

Organic carbon isotopes were measured from whole rock samples collected from the uppermost part of the Penglaitan section, beginning with the terrestrial interval. The $\delta^{13}C_{org}$ values range over 4.5‰, from –29.5‰ to –24.5‰, with much of the early variability likely related to mixing of terrestrial and marine organic materials. In the fully marine part of the section

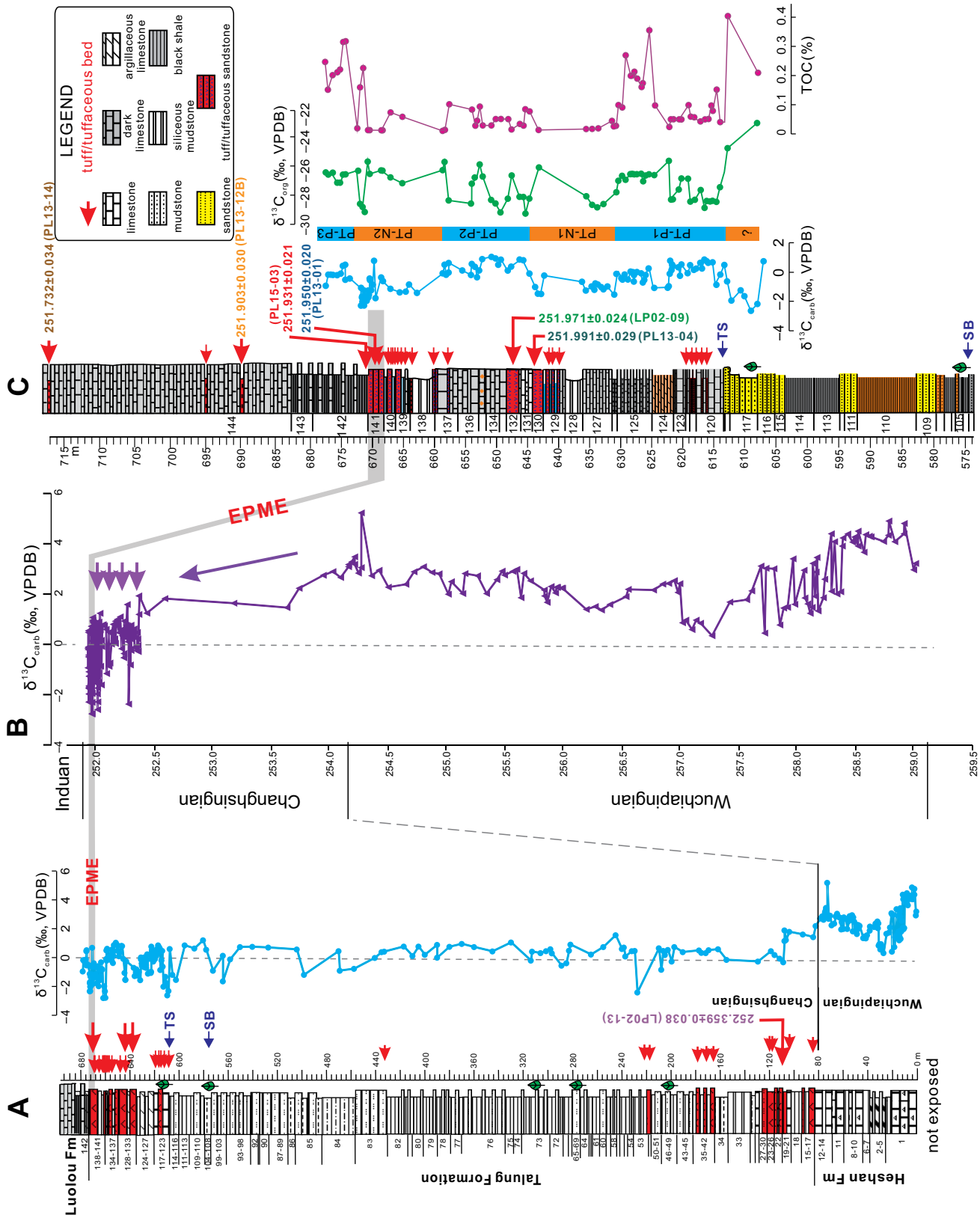

Figure 10. $\delta^{13}C_{carb}$, $\delta^{13}C_{org}$ and TOC (total organic carbon) profiles from the Lopingian (A—scaled to thickness; B—scaled to absolute age) and across the end-Permian mass extinction (EPME) interval (C) at the Penglaitan section. SB—sequence boundary; TS—transgressive surface; VPDB—Vienna Pee Dee belemnite. Arrows indicate negative excursions. Full data are presented in Table DR2 (footnote 1).

above 610 m, $\delta^{13}C_{org}$ values fluctuate between –29‰ and –23‰ (Fig. 10B; Table DR2). Several of the positive excursions correspond to apparent volcanogenic horizons (Fig. 10B), probably suggesting input of terrestrial carbon may have accompanied the tuff. Bed 141 coincides with the onset of a negative excursion of ~2.5‰. This excursion is of similar magnitude to excursions seen in the lower horizons, but is much shorter in duration. Without additional expanded sections for comparison it is difficult to judge whether such excursions reflect global changes or local dynamics. Above Bed 141, $\delta^{13}C_{org}$ values return to the pre-excursion baseline of ~–26‰. Both the $\delta^{13}C_{carb}$ and $\delta^{13}C_{org}$ records from Penglaitan suggest the characteristic PTB negative excursion varies in magnitude and pattern in different sections (Cao et al., 2010; Korte and Kozur, 2010; Shen et al., 2013). Such variations are likely due to either diagenetic overprints on the original $\delta^{13}C$ signals (e.g., Meishan; Li and Jones, 2017) or reflect different sedimentary settings. Most importantly, our data show no correlation at Penglaitan between organic and carbonate carbon isotopes (Fig. 11).

$\delta^{18}O_{apatite}$ OF CONODONTS AND OCEAN PALEOTEMPERATURES

The EPME has been linked to a rapid climate warming of ~8 °C (Brand et al., 2012; Chen et al., 2013; Garbelli et al., 2016; Joachimski et al., 2012; Schobben et al., 2014; Sun et al., 2012). However, the precise temporal relationship between the sudden increase in seawater temperature and the onset of mass extinction has been ambiguous due to the inherent limitations of conventional isotope ratio mass spectrometry (IRMS) methods (i.e., sample size), condensation of the sections (e.g., Meishan, Shangsi and NW Iran) and different sources used (e.g., brachiopods versus conodonts) (Brand et al., 2012; Chen et al., 2016; Garbelli et al., 2016; Joachimski et al., 2012; Schobben et al., 2014). In order to establish a high-resolution paleotemperature profile across the EPME interval, we employed an in situ secondary ion mass spectrometry (SIMS) method to measure oxygen isotopic compositions of conodont apatite ($\delta^{18}O_{apatite}$) from the Penglaitan section, following the standard analytical procedures of the SIMS laboratory (see detailed description of Chen et al., 2016).

We collected more than 100 conodont samples from the uppermost Changhsingian-lowest Triassic interval at Penglaitan. A total of 99 specimens (*Clarkina* sp., n = 71; *Hindeodus* sp., n = 22; ramiform, n = 6) were selected and analyzed. From a technical point of view, ramiforms are not the primary choice for analysis, as they are usually smaller and easily broken when preparing the epoxy mounts. However, the abundance of conodonts around the extinction interval is low, and ramiform elements are usually the only material available in conodont samples. As ramiforms and P1 elements are all parts of the conodont animal dentition (e.g., Purnell et al., 2000), they should reflect common environmental conditions (e.g., seawater temperature). Moreover, previous study of high-resolution data from four sections in South China indicated that the oxygen isotopic values from ramiforms are as reliable as those from *Clarkina* or *Hindeodus* elements (Chen et al., 2016). The oxygen isotopic compositions of seawater, which cannot be measured directly, are another concern for the reliability of oxygen isotope data from conodont apatite and paleotemperature calculations. As explained in a previous study (Chen et al., 2016), we assumed a constant $\delta^{18}O_{seawater}$ at –1‰ (VSMOW, Vienna standard mean ocean water), which is commonly adopted for the "ice-free" period such as the Late Permian–Early Triassic interval. Potential influences from salinity, sea-level change, and pH on $\delta^{18}O_{seawater}$ were probably small compared with the uncertainties of $\delta^{18}O_{apatite}$ analyses using IRMS or SIMS (Chen et al., 2016, p. 33).

Our results (Fig. 12; Table DR3 [footnote 1]) show that: (1) In the upper ~50 m of the Changhsingian (614–665 m), $\delta^{18}O_{apatite}$ values are mostly in the range of 17.0‰ to 18.5‰ (average 17.7‰, n = 43), which is higher than the average post-extinction value of 16.2‰. Three episodes of 3–5 °C temperature fluctuations are temporally consistent with intervals of intensive volcanic activity and the three negative excursions of $\delta^{13}C_{carb}$. (2) A rapid decrease from average 17.7‰ to 16.2‰ in $\delta^{18}O_{apatite}$ values occurred 28 cm above the top of Bed 141. Converting this rapid decrease of 1.5‰ in $\delta^{18}O_{apatite}$ values into relative paleotemperature translates into a substantial warming of 6–8 °C (Lécuyer et al., 2013; Pucéat et al., 2010). If individual samples are considered instead of the long-term average, the sudden drop in $\delta^{18}O_{apatite}$ values at ~671 m suggest an extremely rapid warming event with a magnitude of 10 °C. (3) Measurements on a *Clarkina* specimen 26 cm above the extinction horizon show an average value of 19.0‰ (n = 5), which might indicate a brief cooling episode following the massive volcanic eruption (i.e., Bed 141). More data below this level would be desirable to confirm this brief cooling event, but conodonts are not available

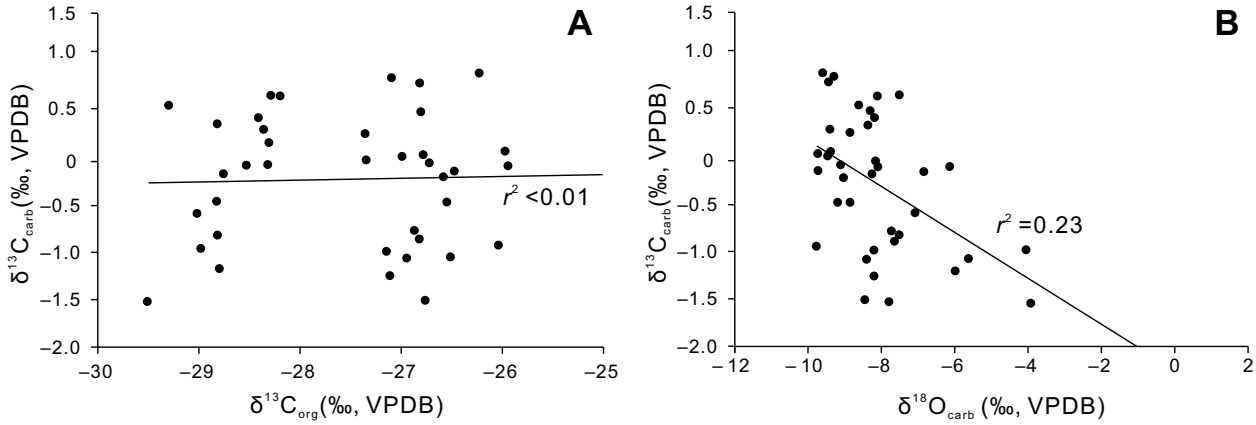

Figure 11. (A) Crossplot of organic carbon versus carbonate carbon isotopes. Note complete lack of correlation, suggesting that remineralized organic C was not diagenetically reincorporated into carbonate. (B) Crossplot of oxygen versus carbon isotopes in carbonate. Weak correlation suggests little to no isotopic exchange with meteoric water. VPDB—Vienna Pee Dee belemnite.

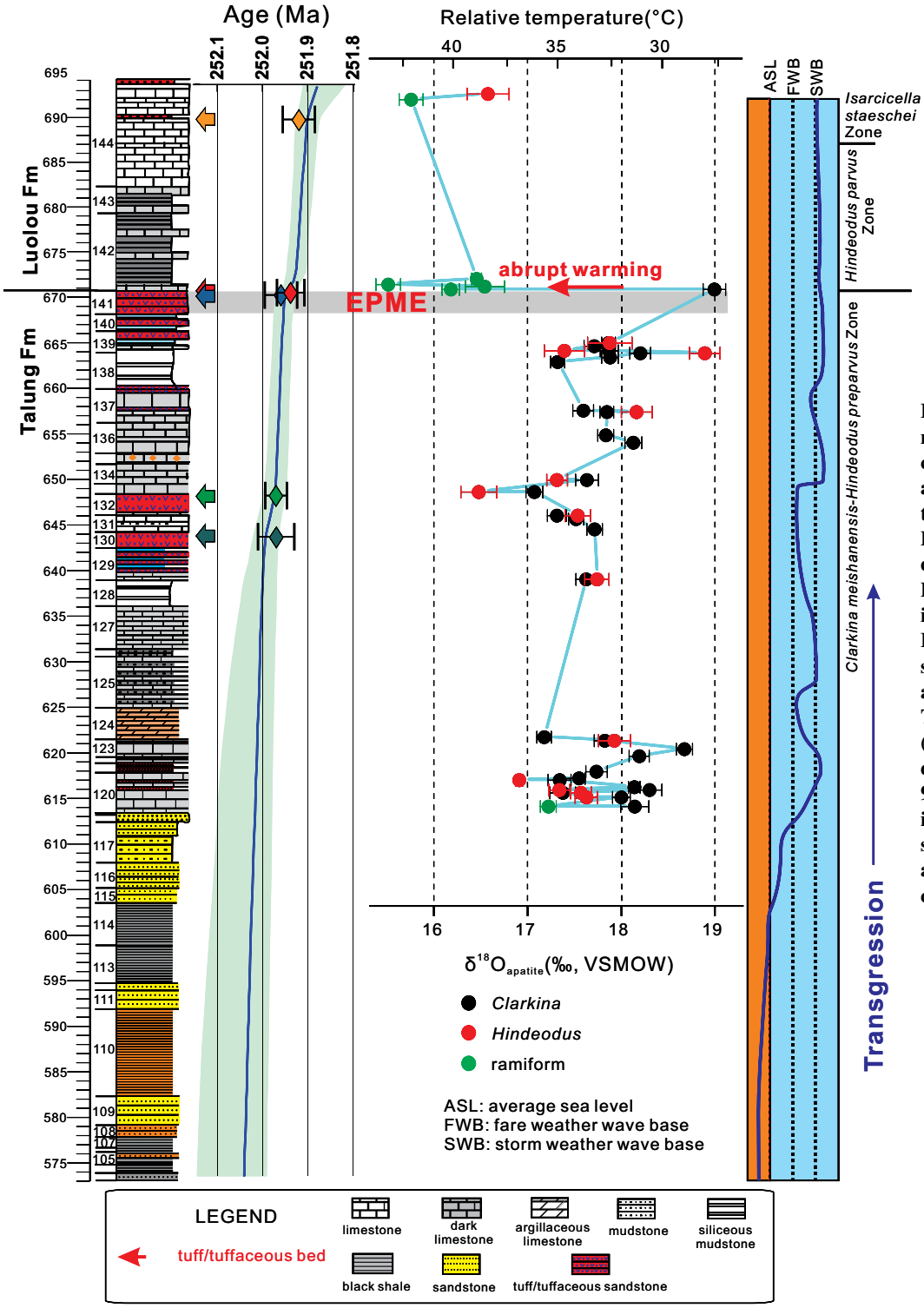

Figure 12. In situ oxygen isotopes measured in conodont apatite and calculated relative temperatures across the end-Permian mass extinction (EPME) interval at the Penglaitan section showing several fluctuations during the latest Permian and an abrupt warming immediately postdating the EPME. Full $\delta^{18}O_{apatite}$ data are presented in Table DR3 (footnote 1), and raw data are presented in Tables DR4–DR6. Dated tuff beds (color-coded), the Bchron age-depth model (blue line), and its 95% error envelope (green shading) are shown to the right of the stratigraphic column (see Table 1 and Fig. 5 for U-Pb geochronological results).

from the tuffaceous deposits (Bed 141; Fig. 12). The timing of this abrupt warming at Penglaitan reinforces previous results indicating a rapid rise in seawater temperatures following the extinction. It slightly postdates the extinction in Bed 141, and also occurs after the extinction in Bed 25, but during the survival interval in Bed 26 at Meishan (Burgess et al., 2014; Chen et al., 2016). It is also noteworthy that $\delta^{18}O_{apatite}$ values from Penglaitan (Fig. 12; Table DR3) are systematically lower than the in situ SIMS results reported from the Meishan, Shangsi, Daijiagou, and Liangfengya sections (Chen et al., 2016). Whether such offsets are related to differences in the environmental setting or color alteration index (CAI: Meishan, ~1 versus Penglaitan, ~3) of conodont elements (Chen et al., 2016; Wheeley et al., 2012) requires further investigation, but somewhat cooler temperatures would be consistent with the deeper water setting at Meishan compared to Penglaitan.

DISCUSSION

Temporal Correlation of the Extinction with Meishan and Other PTB Sections

The uppermost Changhsingian conodonts *Clarkina yini*, *C. meishanensis* and *Hindeodus praeparvus*, as well as the Induan conodonts *Hindeodus parvus*, *Isarcicella staeschei* and *I. isarcica* were recovered from Penglaitan (Fig. 2), which are consistent with the succession of the Meishan section (Brosse et al., 2016; Yuan et al., 2014). The basal thin limestone of Bed 142 immediately above the extinction contains the conodont *Hindeodus praeparvus* and rare specimens of *Clarkina zhejiangensis*, but no other Permian taxa. Abundant foraminifers *Palaeofusulina sinensis*, *Nankinella* sp. and *Colaniella parva* are present in Bed 141 (Fig. 7). The overlying thin-bedded limestone and black shale (Fig. 3) contain the index conodont *Hindeodus parvus*, numerous microgastropod *Polygyrina depressa* and the bivalve *Claraia*. Thus, the conodont biostratigraphy provides a first-order correlation between Meishan and Penglaitan and Bed 141 with the extinction at Penglaitan correlative with Bed 25 at Meishan.

The biostratigraphic correlation between Penglaitan and Meishan is confirmed by high-precision U-Pb geochronology. Our age model equates the tuff layers at 20 cm above Bed 141 (sample PL15-03) and Bed 144 (sample PL13-12B) at Penglaitan, respectively, with weighted mean $^{206}Pb/^{238}U$ dates of 251.939 ± 0.031 Ma and 251.920 ± 0.045 Ma (Table 1; Fig. 5) to Beds 25 and 28 at Meishan, which were dated as 251.941 ± 0.037 Ma and 251.880 ± 0.031 Ma (Burgess et al., 2014). Because the latest U-Pb geochronology from Meishan (Burgess et al., 2014) was determined in the same laboratory and following the same procedures as in this study, the results can be directly compared without having to consider interlaboratory bias (Fig. 2).

Baresel et al. (2017) presented high-precision U-Pb zircon geochronology by the CA-ID-TIMS method from the Penglaitan and Dongpan sections in South China and were the first to apply the Bchron age-depth modeling to the study of the Permian-Triassic successions. They used modern EARTHTIME isotopic tracers and protocols in their analyses and reported an interpolated Permian-Triassic lithostratigraphic boundary age of 251.984 ± 0.031 Ma at Penglaitan. Although the analytical standards, interpolation algorithm and the reported boundary age of Baresel et al. (2017) are consistent with those presented here, there are notable dissimilarities between the two chronostratigraphic models. First, all of the four dated samples of Baresel et al. (2017) occur within a 1.6 m stratigraphic interval near the boundary, as opposed to the 73.5 m span of our six dated samples (excluding our lowermost sample LP02-13). In particular, the three Changhsingian dates of Baresel et al. (2017) fall within the upper half of our Bed 141, an interval of mixed tuffs and tuffaceous sandstones (see "Petrologic examination" above) with a complex zircon age spectrum (see our sample PL13-01, Fig. 5). As a result the estimated sediment accumulation rate of Baresel et al. (2017) for the uppermost Talung Formation (0.7 ± 0.3 cm/k.y.) is as much as two orders of magnitude lower than that of our study. Second, the Baresel et al. (2017) interpolated age of the formation boundary at Penglaitan is strongly influenced by the single age constraint (PEN-22) from above the boundary, whereas the even distribution of age data about the boundary in our study yields a better age-depth model.

Overall, our PTB age model from Penglaitan is fully consistent with that of other investigated PTB sections with high-precision U-Pb geochronology throughout the Nanpanjiang Basin in South China. These include the Dongpan (Baresel et al., 2017) and Taiping (Lehrmann et al., 2015) sections to the southwest and west of Penglaitan, respectively.

Variable Survivability of Permian Taxa

Previous studies of the Meishan GSSP have established that the major extinction event occurred during the deposition of top of Bed 24e and Bed 25, with some relict Permian taxa surviving until Bed 28 (Burgess et al., 2014; Jin et al., 2000; S.Z. Shen et al., 2011a; Sheng et al., 1984; Song et al., 2013). There is disagreement whether this was simply a survival interval or an interval with some biotic recovery, followed by a second extinction pulse at Bed 28. Wang et al. (2014) concluded that it was a single pulse extinction with interpretation differences resolved as an artifact of uneven sampling and facies control. In contrast, at Penglaitan no Permian benthic megafossils have been found above the extinction and into the Early Triassic. This demonstrates the considerable variability among the PTB sections in the diversity and abundance of surviving species, as well as the timing of appearance of the first Triassic taxa (Brosse et al., 2016; Yuan et al., 2015; Zhang et al., 2014). Such variability may be due to fossil preservation, local ecologic conditions, collecting intensity, or more likely different manifestations of the extinction and survival in different sedimentary settings (Figs. 3, 4). Our petrologic study of the lithology of Bed 141 and Bed 142 shows a dramatic change of biological community (between Figs. 7I–7J, 7N and Fig. 7M). For example, the FO of *Isarcicella staeschei* and *I. isarcica* appear slightly earlier at Penglaitan than at Meishan, based on geochronologic calibration. However, the apparent diachroneity of these key species is essentially within the range of U-Pb age uncertainties and could equally be interpreted as simultaneous. High-resolution studies must therefore use all possible correlation tools.

Cause of Extinction and Potential Signals of Early Environmental Degradation

The expanded Penglaitan section provides the resolution necessary for detailed insights into the tempo and pattern of the most severe Phanerozoic collapse of marine ecosystems, insight that is not possible from most previously studied sections. Fossil range data show that a highly diverse marine ecosystem suddenly disappeared during the time of deposition of Bed 141 (Fig. 4). Despite the expanded nature of this section, we see no unequivocal evidence for a decline in faunal diversity prior to the main extinction. The Signor-Lipps effect, with backward-smearing of LOs, is likely responsible for disappearances below the thick tuffaceous flow deposit (Bed 141) at Penglaitan. Thus the LO data are consistent with a single extinction pulse temporally coincident with Bed 141. No typical Permian-type benthic taxa survived the extinction except for the conodont *Hindeodus praeparvus*, but Triassic taxa (*Claraia* cf. *dieneri*) began to occur before the extinction (Figs. 3, 4). Similar patterns showing sudden extinction of Permian taxa have been documented from the Cili section (Wang et al., 2009), sections in the Great Bank of Guizhou (Lehrmann et al., 2015; Payne et al., 2007) and the Waili section in Guangxi (Ovtcharova et al., 2006) and with Bed 25 at Meishan. Thus the most plausible reading of the data is a single major extinction pulse across these sections.

The link between volcanism and the EPME is complicated by the occurrence of widespread regional marginal-arc volcanism in South China. More than 50 volcanic eruptions are recorded from the last ~420 k.y. of the Permian (Figs. 2, 4). Although the sudden extinction coincided with the time of deposition of a thick tuffaceous unit at Penglaitan (Fig. 3), there is no evidence for a causal connection between this regional volcanism in South China and the global extinction.

The Siberian Traps represent one of the most voluminous and abrupt continental volcanic events of the Phanerozoic and have been widely proposed as the most plausible trigger for the EPME (Burgess and Bowring, 2015; Burgess et al., 2017; Campbell et al., 1992; Ivanov et al., 2013; Kamo et al., 2003; Renne et al., 1995). However, the tempo of the extinction based on

studies in South China (e.g., Meishan) (Burgess et al., 2014; Jin et al., 2000; Liu et al., 2017; S.Z. Shen et al., 2011a) is more rapid than the estimated duration of the Siberian Traps volcanism (~1 m.y.) (Burgess and Bowring, 2015; Burgess et al., 2014, 2017). The simplest interpretation would be that the global extinction was driven primarily by the effects of the Siberian volcanic eruptions. However, direct degassing of CO_2 from the Siberian Traps may not have been sufficient to drive the rapid negative 4‰–5‰ $\delta^{13}C$ shift (Berner, 2002; Svensen et al., 2009). The abruptness of the mass extinction event as documented in South China supports the suggestion that a particular phase of global volcanism triggered more extensive environmental effects (e.g., through destruction of coal-bearing, petroleum-bearing, and evaporite deposits to increase CO_2, thermogenic heating of coal to form methane, plus greater release of volcanic sulfates) (Burgess et al., 2017; Erwin, 2006; Grasby et al., 2011; Svensen et al., 2009). This interpretation is supported by the recent Zn isotope evidence (Liu et al., 2017), which indicates intensive magmatism immediately before the extinction at Bed 25 of Meishan, and the same excursion has been found in the Alps and southern Tibet (Liu Sheng-Ao, 2017 personal commun.).

Paleontological study of most mass extinction intervals has focused on taxonomic diversity, with relatively less attention paid to indications of the ecological dynamics of component communities prior to the extinction. The greatly expanded section at Penglaitan provides an opportunity to examine these dynamics. Increased volcanism began about 300–420 k.y. before the extinction in both South China and Siberia. It has been proposed that the increased volcanism may have initiated disruption of the marine ecosystem (e.g., Burgess et al., 2017), diminished ecological resilience, and declines in species abundances and thus ecological function without initially triggering major diversity drop. Some less resilient communities (e.g., in Arctic Canada, see Algeo et al., 2012) may have shown earlier declines in diversity. Although we do not report well-sampled abundance data from the Penglaitan section in this paper, several factors suggest the importance of conducting such research in the future.

Possible evidence of environmental degradation prior to the extinction event include: First, a gradual depletion of $\delta^{13}C_{carb}$ at Meishan beginning ~60 k.y. before deposition of Bed 25 and associated with a distinct negative excursion of $\delta^{66}Zn$ at Meishan, and 2‰–3‰ positive and negative excursions in $\delta^{13}C_{carb}$, $\delta^{13}C_{org}$ in the expanded Penglaitan section prior to the sudden collapse of the ecosystem (Burgess et al., 2014; Cao et al., 2009; Liu et al., 2017; Y. Shen et al., 2011b; Xie et al., 2007), signaling the onset of environmental stress. Second, recent analyses of biodiversity through the entire Lopingian, and across the PTB in South China and the peri-Gondwanan region, reveal increased extinction rates and decreased di-

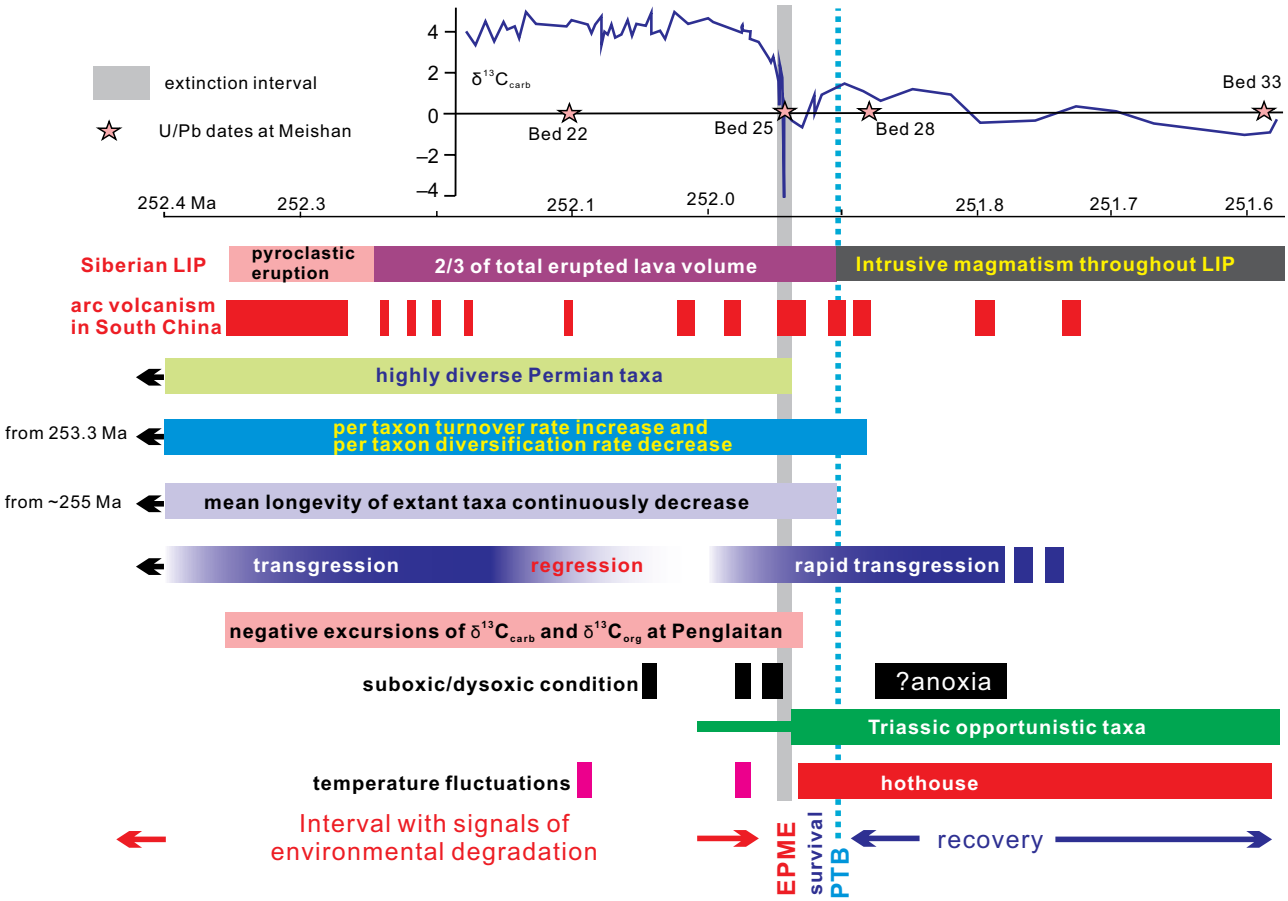

Figure 13. Summary of the global geologic, paleobiologic and ocean chemical events associated with the Permian-Triassic boundary (PTB) interval mapped onto the Meishan Global Stratotype Section and Point. Meishan geochronology and carbon isotope record from Burgess et al. (2014). U-Pb ages for the Siberian Traps from Burgess and Bowring (2015). Grey line and the blue dashed line signify the end-Permian mass extinction interval and the Permian-Triassic boundary, respectively. EPME—end-Permian mass extinction; LIP—large igneous province.

versification rates before the EPME (Wang et al., 2014). In addition, there was a steady decline in mean species longevity from the middle Wuchiapingian that reached a tipping point around the middle Changhsingian (see fig. 4 of Wang et al., 2014), possibly reflecting increased environmental stress. Third, a reduction in body size (Lilliput effect) in brachiopods (He et al., 2015) and high abundance of the Early Triassic progenitor taxon *Claraia* cf. *dieneri* (Figs. 4, 8) prior to the extinction interval at Penglaitan may also indicate the onset of environmental stress. Fourth, fluctuations in ocean paleotemperature (3–5 °C; Fig. 12), and regional euxinic or anoxic conditions (Cao et al., 2009; Y. Shen et al., 2011b) characterize the interval before the EPME (Fig. 13). This evidence suggests increased environmental pressures on marine communities during the latest Changhsingian Stage. Progressive environmental deterioration in northwestern Pangea prior to the end-Permian extinction has also been discussed (Grasby et al., 2015), but events like the loss of carbonate benthos (e.g., lysocline shoaling) seem to precede those in South China. While these indicators support early environmental stress, testing this hypothesis will require more extensive collection of abundance data from Penglaitan and analysis of the structure of ecological networks from late Changhsingian through the extinction interval based on more expanded sections in different regions.

CONCLUSION

High-precision U-Pb geochronology, biostratigraphy, and chemostratigraphy from the highly expanded section at Penglaitan, Guangxi, South China, reveal a sudden end-Permian mass extinction at 251.939 ± 0.031 Ma. The extinction is marked by a dramatic biotic change from a highly diverse Permian benthic-dominated community to a low-diversity Triassic micro-gastropod and bivalve-dominated community, which occurred coincident with deposition of a massive tuffaceous unit that was accumulated within 31 ± 31 k.y. The geologically instantaneous extinction horizon is temporally consistent with the major extinction pulse at Bed 25 of Meishan and globally correlative with that documented in most other sections around the world. Despite extensive collecting, no Permian-type species persist into the earliest Triassic at Penglaitan, which suggests that the survivability of Permian taxa is variable and dependent upon the severity of environmental perturbation in different environmental settings. The suddenness of the extinction shown by Penglaitan and many other sections in South China appears to fit a scenario in which the onset of Siberian Traps and South China intensive arc volcanism ~420 k.y. before the extinction significantly reduced the stability of the ecosystem to the point when a single event could lead to its collapse. A major event at 251.939 ± 0.031 Ma finally resulted in a sudden collapse of the ecosystem at the end-Permian mass extinction at Meishan and Penglaitan.

ACKNOWLEDGMENTS

This work was supported by the Strategic Priority Research Program (B) (XDB26000000, XDB18000000), and the Key Research Program of Frontier Sciences (QYZDY-SSW-DQC023) of the Chinese Academy of Sciences. C.M.H. and S.D.S. acknowledge support from a NSERC Discovery Grant. We thank Ryan Frazer (Massachusetts Institute of Technology) for Bchron simulations, Hugo Bucher (Universität Zürich [UZH]), Seth D. Burgess (U.S. Geological Survey), and other anonymous reviewers for their comments that have improved this manuscript.

REFERENCES CITED

Algeo, T., Henderson, C.M., Ellwood, B., Rowe, H., Elswick, E., Bates, S., Lyons, T., Hower, J.C., Smith, C., Maynard, B., Hays, L.E., Summons, R.E., Fulton, J., and Freeman, K.H., 2012, Evidence for a diachronous Late Permian marine crisis from the Canadian Arctic region: Geological Society of America Bulletin, v. 124, p. 1424–1448, https://doi.org/10.1130/B30505.1.

Baresel, B., Bucher, H., Brosse, M., Cordey, F., Guodun, K., and Schaltegger, U., 2017, Precise age for the Permian–Triassic boundary in South China from high-precision U-Pb geochronology and Bayesian age–depth modeling: Solid Earth, v. 8, p. 361–378, https://doi.org/10.5194/se-8-361-2017.

Berner, R.A., 2002, Examination of hypotheses for the Permo-Triassic boundary extinction by carbon cycle modeling: Proceedings of the National Academy of Sciences of the United States of America, v. 99, p. 4172–4177, https://doi.org/10.1073/pnas.032095199.

Brand, U., Posenato, R., Came, R., Affek, H., Angiolini, L., Azmy, K., and Farabegoli, E., 2012, The end-Permian mass extinction: A rapid volcanic CO_2 and CH_4-climatic catastrophe: Chemical Geology, v. 322–323, p. 121–144, https://doi.org/10.1016/j.chemgeo.2012.06.015.

Brookfield, M.E., Twitchett, R.J., and Goodings, C., 2003, Palaeoenvironments of the Permian-Triassic transition sections in Kashmir, India: Palaeogeography, Palaeoclimatology, Palaeoecology, v. 198, p. 353–371, https://doi.org/10.1016/S0031-0182(03)00476-0.

Brosse, M., Bucher, H., and Goudemand, N., 2016, Quantitative biochronology of the Permian–Triassic boundary in South China based on conodont unitary associations: Earth-Science Reviews, v. 155, p. 153–171, https://doi.org/10.1016/j.earscirev.2016.02.003.

Burgess, S.D., and Bowring, S.A., 2015, High-precision geochronology confirms voluminous magmatism before, during, and after Earth's most severe extinction: Science Advances, v. 1, p. e1500470, https://doi.org/10.1126/sciadv.1500470.

Burgess, S.D., Bowring, S.A., and Shen, S.Z., 2014, High-precision timeline for Earth's most severe extinction: Proceedings of the National Academy of Sciences of the United States of America, v. 111, p. 3316–3321, https://doi.org/10.1073/pnas.1317692111 (erratum at http://doi.org/10.1073/pnas.1403228111).

Burgess, S.D., Muirhead, J.D., and Bowring, S.A., 2017, Initial pulse of Siberian Traps sills as the trigger of the end-Permian mass extinction: Nature Communications, v. 8, p. 164, https://doi.org/10.1038/s41467-017-00083-9.

Campbell, I.H., Czamanske, G.K., Fedorenko, V.A., Hill, R.I., and Stepanov, V., 1992, Synchronism of the Siberian Traps and the Permian-Triassic boundary: Science, v. 258, p. 1760–1763, https://doi.org/10.1126/science.258.5089.1760.

Cao, C.Q., and Zheng, Q.F., 2007, High-resolution lithostratigraphy of the Changhsingian Stage in Meishan section D, Zhejiang: Journal of Stratigraphy, v. 31, p. 14–22.

Cao, C.Q., and Zheng, Q.F., 2009, Geological event sequences of the Permian-Triassic transition recorded in the microfacies in Meishan section: Science in China, Series D, Earth Sciences, v. 52, no. 10, p. 1529–1536, https://doi.org/10.1007/s11430-009-0113-0.

Cao, C.Q., Wang, W., and Jin, Y.G., 2002, Carbon isotope excursions across the Permian-Triassic boundary in the Meishan section, Zhejiang Province, China: Chinese Science Bulletin, v. 47, p. 1125–1129, https://doi.org/10.1360/02tb9252.

Cao, C.Q., Love, G.D., Hays, L.E., Wang, W., Shen, S.Z., and Summons, R.E., 2009, Biogeochemical evidence for euxinic oceans and ecological disturbance presaging the end-Permian mass extinction event: Earth and Planetary Science Letters, v. 281, p. 188–201, https://doi.org/10.1016/j.epsl.2009.02.012.

Cao, C.Q., Yang, Y.C., Shen, S.Z., Wang, W., Zheng, Q.F., and Summons, R.E., 2010, Pattern of $\delta^{13}C_{carb}$ and implications for geological events during the Permian-Triassic transition in South China: Geological Journal, v. 45, p. 186–194, https://doi.org/10.1002/gj.1220.

Chen, B., Joachimski, M.M., Shen, S.Z., Lambert, L.L., Lai, X.L., Wang, X.D., Chen, J., and Yuan, D.X., 2013, Permian ice volume and palaeoclimate history: Oxygen isotope proxies revisited: Gondwana Research, v. 24, p. 77–89, https://doi.org/10.1016/j.gr.2012.07.007.

Chen, J., Shen, S.Z., Li, X.H., Xu, Y.G., Joachimski, M.M., Bowring, S.A., Erwin, D.H., Yuan, D.X., Chen, B., Zhang, H., Wang, Y., Cao, C.Q., Zheng, Q.F., and Mu, L., 2016, High-resolution SIMS oxygen isotope analysis on conodont apatite from South China and implications for the end-Permian mass extinction: Palaeogeography, Palaeoclimatology, Palaeoecology, v. 448, p. 26–38, https://doi.org/10.1016/j.palaeo.2015.11.025.

Ehiro, M., and Shen, S.Z., 2010, Ammonoid succession across the Wuchiapingian/Changhsingian boundary of the northern Penglaitan Section in the Laibin area, Guangxi, South China: Geological Journal, v. 45, p. 162–169, https://doi.org/10.1002/gj.1228.

Erwin, D.H., 2006, Extinction: How life on Earth nearly ended 250 million years ago: New Jersey, Princeton University Press, 296 p.

Garbelli, C., Angiolini, L., Brand, U., Shen, S.Z., Jadoul, F., Posenato, R., Azmy, K., and Cao, C.Q., 2016, Neotethys seawater chemistry and temperature at the dawn of the end Permian mass extinction: Gondwana Research, v. 35, p. 272–285, https://doi.org/10.1016/j.gr.2015.05.012.

Grasby, S.E., and Beauchamp, B., 2009, Latest Permian to Early Triassic basin-to-shelf anoxia in the Sverdrup Basin, Arctic Canada: Chemical Geology, v. 264, p. 232–246, https://doi.org/10.1016/j.chemgeo.2009.03.009.

Grasby, S.E., Sanei, H., and Beauchamp, B., 2011, Catastrophic dispersion of coal fly ash into oceans during the latest Permian extinction: Nature Geoscience, v. 4, p. 104–107, https://doi.org/10.1038/ngeo1069.

Grasby, S.E., Beauchamp, B., Bond, D.P.G., Wignall, P., Talavera, C., Galloway, J.M., Piepjohn, K., Reinhardt, L., and Blomeier, D., 2015, Progressive environmental deterioration in northwestern Pangea leading to the latest Permian extinction: Geological Society of America Bulletin, v. 127, p. 1331–1347, https://doi.org/10.1130/B31197.1.

Haslett, J., and Parnell, A., 2008, A simple monotone process with application to radiocarbon-dated depth chronologies: Journal of the Royal Statistical Society, Series C, Applied Statistics, v. 57, p. 399–418, https://doi.org/10.1111/j.1467-9876.2008.00623.x.

Hays, L.E., Grice, K., Foster, C.B., and Summons, R.E., 2012, Biomarker and isotopic trends in a Permian–Tri-

assic sedimentary section at Kap Stosch, Greenland: Organic Geochemistry, v. 43, p. 67–82, https://doi.org/10.1016/j.orggeochem.2011.10.010.

He, B., Zhong, Y.T., Xu, Y.G., and Li, X.H., 2014, Triggers of Permo-Triassic boundary mass extinction in South China: The Siberian Traps or Paleo-Tethys ignimbrite flare-up?: Lithos, v. 204, p. 258–267, https://doi.org/10.1016/j.lithos.2014.05.011.

He, W.H., Shi, G.R., Twitchett, R.J., Zhang, Y., Zhang, K.X., Song, H.J., Yue, M.L., Wu, S.B., Wu, H.T., Yang, T.L., and Xiao, Y.F., 2015, Late Permian marine ecosystem collapse began in deeper waters: evidence from brachiopod diversity and body size changes: Geobiology, v. 13, p. 123–138, https://doi.org/10.1111/gbi.12119.

Hermann, E., Hochuli, P.A., Bucher, H., Vigran, J.O., Weissert, H., and Bernasconi, S.M., 2010, A close-up view of the Permian–Triassic boundary based on expanded organic carbon isotope records from Norway (Trøndelag and Finnmark Platform): Global and Planetary Change, v. 74, p. 156–167, https://doi.org/10.1016/j.gloplacha.2010.10.007.

Holser, W.T., Schonlaub, H.P., Attrep, M., Boeckelmann, K., Klein, P., Magaritz, M., Orth, C.J., Fenninger, A., Jenny, C., Kralik, M., Mauritsch, H., Pak, E., Schramm, J.M., Stattegger, K., and Schmoller, R., 1989, A unique geochemical record at the Permian/Triassic boundary: Nature, v. 337, p. 39–44, https://doi.org/10.1038/337039a0.

Ivanov, A.V., He, H.Y., Yan, L.K., Ryabov, V.V., Shevko, A.Y., Palesskii, S.V., and Nikolaeva, I.V., 2013, Siberian Traps large igneous province: Evidence for two flood basalt pulses around the Permo-Triassic boundary and in the Middle Triassic, and contemporaneous granitic magmatism: Earth-Science Reviews, v. 122, p. 58–76, https://doi.org/10.1016/j.earscirev.2013.04.001.

Jin, Y.G., Mei, S.L., Wang, W., Wang, X.D., Shen, S.Z., Shang, Q.H., and Chen, Z.Q., 1998, On the Lopingian Series of the Permian System, *in* Jin, Y.G., Wardlaw, B.R., and Wang, Y., eds., Permian stratigraphy, environments and resources: Hefei, China University of Science and Technology Press, Palaeoworld 9, v. 2, p. 1–18.

Jin, Y.G., Wang, Y., Wang, W., Shang, Q.H., Cao, C.Q., and Erwin, D.H., 2000, Pattern of marine mass extinction near the Permian-Triassic boundary in South China: Science, v. 289, p. 432–436, https://doi.org/10.1126/science.289.5478.432.

Jin, Y.G., Shen, S.Z., Henderson, C.M., Wang, X.D., Wang, W., Wang, Y., Cao, C.Q., and Shang, Q.H., 2006, The Global Stratotype Section and Point (GSSP) for the boundary between the Capitanian and Wuchiapingian stage (Permian): Episodes, v. 29, p. 253–262.

Joachimski, M.M., Lai, X.L., Shen, S.Z., Jiang, H.S., Luo, G.M., Chen, B., Chen, J., and Sun, Y.D., 2012, Climate warming in the latest Permian and the Permian–Triassic mass extinction: Geology, v. 40, p. 195–198, https://doi.org/10.1130/G32707.1.

Kamo, S.L., Czamanske, G.K., Amelin, Y., Fedorenko, V.A., Davis, D.W., and Trofimov, V.R., 2003, Rapid eruption of Siberian flood-volcanic rocks and evidence for coincidence with the Permian-Triassic boundary and mass extinction at 251 Ma: Earth and Planetary Science Letters, v. 214, p. 75–91, https://doi.org/10.1016/S0012-821X(03)00347-9.

Korte, C., and Kozur, H.W., 2010, Carbon-isotope stratigraphy across the Permian-Triassic boundary: A review: Journal of Asian Earth Sciences, v. 39, p. 215–235, https://doi.org/10.1016/j.jseaes.2010.01.005.

Lécuyer, C., Amiot, R., Touzeau, A., and Trotter, J., 2013, Calibration of the phosphate $\delta^{18}O$ thermometer with carbonate–water oxygen isotope fractionation equations: Chemical Geology, v. 347, p. 217–226, https://doi.org/10.1016/j.chemgeo.2013.03.008.

Lehrmann, D.J., Enos, P., Payne, J.L., Montgomery, P., Wei, J.Y., Yu, Y., Xiao, J.F., and Orchard, M.J., 2005, Permian and Triassic depositional history of the Yangtze platform and Great Bank of Guizhou in the Nanpanjiang basin of Guizhou and Guangxi, south China: Albertiana, v. 33, p. 149–168.

Lehrmann, D.J., Stepchinski, L., Altiner, D., Orchard, M.J., Montgomery, P., Enos, P., Ellwood, B.B., Bowring, S.A., Ramezani, J., Wang, H., Wei, J., Yu, M., Griffiths, J.D., Minzoni, M., Schaal, E.K., Li, X., Meyer, K.M., and Payne, J.L., 2015, An integrated biostratigraphy (conodonts and foraminifers) and chronostratigraphy (paleomagnetic reversals, magnetic susceptibility, elemental chemistry, carbon isotopes and geochronology) for the Permian–Upper Triassic strata of Guandao section, Nanpanjiang Basin, south China: Journal of Asian Earth Sciences, v. 108, p. 117–135, https://doi.org/10.1016/j.jseaes.2015.04.030.

Li, R., and Jones, B., 2017, Diagenetic overprint on negative $\delta^{13}C$ excursions across the Permian/Triassic boundary: A case study from Meishan section, China: Palaeogeography, Palaeoclimatology, Palaeoecology, v. 468, p. 18–33, https://doi.org/10.1016/j.palaeo.2016.11.044.

Liu, S.A., Wu, H.C., Shen, S.Z., Jiang, G.Q., Zhang, S.H., Lv, Y.W., Zhang, H., and Li, S.G., 2017, Zinc isotope evidence for intensive magmatism immediately before the end-Permian mass extinction: Geology, v. 45, p. 343–346, https://doi.org/10.1130/G38644.1.

Ovtcharova, M., Bucher, H., Schaltegger, U., Galfetti, T., Brayard, A., and Guex, J., 2006, New Early to Middle Triassic U-Pb ages from South China: Calibration with ammonoid biochronozones and implications for the timing of the Triassic biotic recovery: Earth and Planetary Science Letters, v. 243, p. 463–475, https://doi.org/10.1016/j.epsl.2006.01.042.

Pakistani-Japanese Working Group, 1985, Permian and Triassic Systems in the Salt Range and Surghar Range, Pakistan, *in* Nakazawa, K., and Dickins, J.M., eds., "The Tethys": Her paleogeography and paleobiogeography from Paleozoic to Mesozoic: Tokyo, Tokai University Press, p. 221–312.

Parnell, A.C., Haslett, J., Allen, J.R.M., Buck, C.E., and Huntley, B., 2008, A flexible approach to assessing synchroneity of past events using Bayesian reconstructions of sedimentation history: Quaternary Science Reviews, v. 27, no. 19-20, p. 1872–1885, https://doi.org/10.1016/j.quascirev.2008.07.009.

Payne, J.L., Lehrmann, D.J., Follett, D., Seibel, M., Kump, L.R., Riccardi, A., Altiner, D., Sano, H., and Wei, J., 2007, Erosional truncation of uppermost Permian shallow-marine carbonates and implications for Permian-Triassic boundary events: Geological Society of America Bulletin, v. 119, p. 771–784, https://doi.org/10.1130/B26091.1.

Perri, M.C., and Farabegoli, F., 2003, Conodonts across the Permian-Triassic boundary in the Southern Alps: Courier Forschungs Institut Senckenberg, v. 245, p. 281–313.

Posenato, R., 2010, Marine biotic events in the Lopingian succession and latest Permian extinction in the Southern Alps (Italy): Geological Journal, v. 45, p. 195–215, https://doi.org/10.1002/gj.1212.

Pucéat, E., Joachimski, M.M., Bouilloux, A., Monna, F., Bonin, A., Motreuil, S., Morinière, P., Hénard, S., Mourin, J., Dera, G., and Quesne, D., 2010, Revised phosphate–water fractionation equation reassessing paleotemperatures derived from biogenic apatite: Earth and Planetary Science Letters, v. 298, p. 135–142, https://doi.org/10.1016/j.epsl.2010.07.034.

Purnell, M.A., Donoghue, P.C.J., and Aldridge, R.J., 2000, Orientation and anatomical notation in conodonts: Journal of Paleontology, v. 74, p. 113–122, https://doi.org/10.1017/S0022336000031292.

Rampino, M.R., Prokoph, A., and Adler, A., 2000, Tempo of the end-Permian event: high-resolution cyclostratigraphy at the Permian-Triassic boundary: Geology, v. 28, p. 643–646, https://doi.org/10.1130/0091-7613(2000)28<643:TOTEEH>2.0.CO;2.

Renne, P.R., Zhang, Z.C., Richards, M.A., Black, M.T., and Basu, A.R., 1995, Synchrony and causal relations between Permian-Triassic boundary crises and Siberian flood volcanism: Science, v. 269, p. 1413–1416, https://doi.org/10.1126/science.269.5229.1413.

Schobben, M., Joachimski, M.M., Korn, D., Leda, L., and Korte, C., 2014, Palaeotethys seawater temperature rise and an intensified hydrological cycle following the end-Permian mass extinction: Gondwana Research, v. 26, p. 675–683, https://doi.org/10.1016/j.gr.2013.07.019.

Shen, S.Z., and Bowring, S.A., 2014, The end-Permian mass extinction: a still unexplained catastrophe: National Science Review, v. 1, p. 492–495, https://doi.org/10.1093/nsr/nwu047.

Shen, S.Z., Cao, C.Q., Zhang, H., Bowring, S.A., Henderson, C.M., Payne, J.L., Davydov, V.I., Chen, B., Yuan, D.X., Zhang, Y.C., Wang, W., and Zheng, Q.F., 2013, High-resolution $\delta^{13}C_{carb}$ chemostratigraphy from latest Guadalupian through earliest Triassic in South China and Iran: Earth and Planetary Science Letters, v. 375, p. 156–165, https://doi.org/10.1016/j.epsl.2013.05.020.

Shen, S.Z., Wang, Y., Henderson, C.M., Cao, C.Q., and Wang, W., 2007, Biostratigraphy and lithofacies of the Permian System in the Laibin-Heshan area of Guangxi, South China: Palaeoworld, v. 16, p. 120–139, https://doi.org/10.1016/j.palwor.2007.05.005.

Shen, S.Z., Henderson, C.M., Bowring, S.A., Cao, C.Q., Wang, Y., Wang, W., Zhang, H., Zhang, Y.C., and Mu, L., 2010, High-resolution Lopingian (Late Permian) timescale of South China: Geological Journal, v. 45, p. 122–134, https://doi.org/10.1002/gj.1232.

Shen, S.Z., Crowley, J.L., Wang, Y., Bowring, S.A., Erwin, D.H., Sadler, P.M., Cao, C.Q., Rothman, D.H., Henderson, C.M., Ramezani, J., Zhang, H., Shen, Y., Wang, X.D., Wang, W., Mu, L., Li, W.Z., Tang, Y.G., Liu, X.L., Liu, L.J., Zeng, Y., Jiang, Y.F., and Jin, Y.G., 2011a, Calibrating the end-Permian mass extinction: Science, v. 334, p. 1367–1372, https://doi.org/10.1126/science.1213454.

Shen, Y., Farquhar, J., Zhang, H., Masterson, A., Zhang, T.G., and Wing, B.A., 2011b, Multiple S-isotopic evidence for episodic shoaling of anoxic water during Late Permian mass extinction: Nature Communications, v. 2, p. 1–5, https://doi.org/10.1038/ncomms1217.

Sheng, J.Z., Chen, C.Z., Wang, Y.G., Rui, L., Liao, Z.T., Bando, Y., Ishii, K.I., Nakazawa, K., and Nakamura, K., 1984, Permian-Triassic boundary in middle and eastern Tethys: Journal of the Faculty of Science, Hokkaido University, Series 4: Geology and Mineralogy, v. 21, p. 133–181.

Song, H.J., Tong, J.N., and Chen, Z.Q., 2009, Two episodes of foraminiferal extinction near the Permian–Triassic boundary at the Meishan section, South China: Australian Journal of Earth Sciences, v. 56, p. 765–773, https://doi.org/10.1080/08120090903002599.

Song, H.J., Wignall, P.B., Tong, J.N., and Yin, H.F., 2013, Two pulses of extinction during the Permian-Triassic crisis: Nature Geoscience, v. 6, p. 52–56, https://doi.org/10.1038/ngeo1649.

Sun, Y.D., Joachimski, M.M., Wignall, P.B., Yan, C.B., Chen, Y.L., Jiang, H.S., Wang, L., and Lai, X.L., 2012, Lethally hot temperatures during the Early Triassic greenhouse: Science, v. 338, p. 366–370, https://doi.org/10.1126/science.1224126.

Svensen, H., Planke, S., Polozov, A.G., Schmidbauer, N., Corfu, F., Podladchikov, Y.Y., and Jamtveit, B., 2009, Siberian gas venting and the end-Permian environmental crisis: Earth and Planetary Science Letters, v. 277, p. 490–500, https://doi.org/10.1016/j.epsl.2008.11.015.

Twitchett, R.J., Looy, C.V., Morante, R., Visscher, H., and Wignall, P.B., 2001, Rapid and synchronous collapse of marine and terrestrial ecosystems during the end-Permian biotic crisis: Geology, v. 29, p. 351–354, https://doi.org/10.1130/0091-7613(2001)029<0351:RASCOM>2.0.CO;2.

Wang, Q.X., Tong, J.N., Song, H.J., and Yang, H., 2009, Ecological evolution across the Permian/Triassic boundary at the Kangjiaping Section in Cili County, Hunan Province, China: Science in China, Series D, Earth Sciences, v. 52, p. 797–806, https://doi.org/10.1007/s11430-009-0077-0.

Wang, Y., Sadler, P.M., Shen, S.Z., Erwin, D.H., Zhang, Y.C., Wang, X.D., Wang, W., Crowley, J.L., and Henderson, C.M., 2014, Quantifying the process and abruptness of the end-Permian mass extinction: Paleobiology, v. 40, p. 113–129, https://doi.org/10.1666/13022.

Wheeley, J.R., Smith, M.P., and Boomer, I., 2012, Oxygen isotope variability in conodonts: implications

for reconstructing Palaeozoic palaeoclimates and palaeoceanography: Journal of the Geological Society, v. 169, p. 239–250, https://doi.org/10.1144/0016-76492011-048.

Wignall, P.B., and Twitchett, R.J., 2002, Permian-Triassic sedimentology of Jameson Land, East Greenland: incised submarine channels in an anoxic basin: Journal of the Geological Society, v. 159, p. 691–703, https://doi.org/10.1144/0016-764900-120.

Xie, S.C., Pancost, R.D., Huang, J.H., Wignall, P.B., Yu, J.X., Tang, X.Y., Chen, L., Huang, X.Y., and Lai, X.L., 2007, Changes in the global carbon cycle occurred as two episodes during the Permian-Triassic crisis: Geology, v. 35, p. 1083–1086, https://doi.org/10.1130/G24224A.1.

Yang, J.H., Cawood, P.A., Du, Y.S., Huang, H., Huang, H.W., and Tao, P., 2012, Large Igneous Province and magmatic arc sourced Permian–Triassic volcanogenic sediments in China: Sedimentary Geology, v. 261–262, p. 120–131, https://doi.org/10.1016/j.sedgeo.2012.03.018.

Yin, H.F., Xie, S.C., Luo, G.M., Algeo, T.J., and Zhang, K.X., 2012, Two episodes of environmental change at the Permian–Triassic boundary of the GSSP section Meishan: Earth-Science Reviews, v. 115, p. 163–172, https://doi.org/10.1016/j.earscirev.2012.08.006.

Yuan, D.X., Shen, S.Z., Henderson, C.M., Chen, J., Zhang, H., and Feng, H.Z., 2014, Revised conodont-based integrated high-resolution timescale for the Changhsingian Stage and end-Permian extinction interval at the Meishan sections, South China: Lithos, v. 204, p. 220–245, https://doi.org/10.1016/j.lithos.2014.03.026.

Yuan, D.X., Chen, J., Zhang, Y.C., Zheng, Q.F., and Shen, S.Z., 2015, Changhsingian conodont succession and the end-Permian mass extinction event at the Daijiagou section in Chongqing, Southwest China: Journal of Asian Earth Sciences, v. 105, p. 234–251, https://doi.org/10.1016/j.jseaes.2015.04.002.

Zhang, Y., Zhang, K.X., Shi, G.R., He, W.H., Yuan, D.X., Yue, M.L., and Yang, T.L., 2014, Restudy of conodont biostratigraphy of the Permian–Triassic boundary section in Zhongzhai, southwestern Guizhou Province, South China: Journal of Asian Earth Sciences, v. 80, p. 75–83, https://doi.org/10.1016/j.jseaes.2013.10.032.

Zheng, Q.F., Cao, C.Q., and Zhang, M.Y., 2013, Sedimentary features of the Permian-Triassic boundary sequence of the Meishan section in Changxing County, Zhejiang Province: Science China, Earth Sciences, v. 56, p. 956–969, https://doi.org/10.1007/s11430-013-4602-9.

Science Editor: Aaron J. Cavosie
Associate Editor: Fernando Corfu

Manuscript Received 14 August 2017
Revised Manuscript Received 9 February 2018
Manuscript Accepted 13 June 2018

Printed in the USA